NASA-CR-192281

Final Report
for the period January 1, 1990 - June 30, 1992

on

ANALYSIS OF ELECTROMAGNETIC INTERFERENCE FROM POWER SYSTEM PROCESSING AND TRANSMISSION COMPONENTS FOR SPACE STATION FREEDOM

Grant No. NAG3-1126

G/...
/N - /8 -CR
/4 3/0 5
P./0/

by

Peter W. Barber
Principal Investigator

and

Nabeel A.O. Demerdash
Co-Principal Investigator

Research Assistants: R. Wang, B. Hurysz, Z. Luo

Department of Electrical and Computer Engineering
Clarkson University
Potsdam, NY 13699-5720

Consultants: Hugh W. Denny, David P. Millard, R. Herkert
Georgia Tech Research Institute

Submitted to

Power Management and Distribution Systems Branch
Mail Stop 500-102
NASA - Lewis Research Center
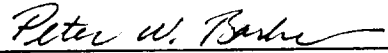21000 Brookpark Road
Cleveland, OH 44135

Final Report
for the period January 1, 1990 - June 30, 1992

on

ANALYSIS OF ELECTROMAGNETIC INTERFERENCE FROM POWER SYSTEM PROCESSING AND TRANSMISSION COMPONENTS FOR SPACE STATION FREEDOM

Grant No. NAG3-1126

by

Peter W. Barber

Peter W. Barber
Principal Investigator

and

Nabeel A.O. Demerdash

Nabeel A.O. Demerdash
Co-Principal Investigator

Research Assistants: R. Wang, B. Hurysz, Z. Luo

Department of Electrical and Computer Engineering
Clarkson University
Potsdam, NY 13699-5720

Consultants: Hugh W. Denny, David P. Millard, R. Herkert
Georgia Tech Research Institute

ii

ANALYSIS OF ELECTROMAGNETIC INTERFERENCE FROM POWER SYSTEM PROCESSING AND TRANSMISSION COMPONENTS FOR SPACE STATION FREEDOM

Table of Contents

List of Figures

List of Tables

Appendices

ANALYSIS OF ELECTROMAGNETIC INTERFERENCE FROM POWER SYSTEM PROCESSING AND TRANSMISSION COMPONENTS FOR SPACE STATION FREEDOM

1 Introduction

The goal of this research project was to analyze the potential effects of electromagnetic interference (EMI) originating from power system processing and transmission components for Space Station Freedom. The approach consists of four steps:

1. Develop analytical tools (models and computer programs).
2. Conduct parameterization (what if?) studies.
3. Predict the global space station EMI environment.
4. Provide a basis for modification of EMI standards.

This report along with previous interim reports constitutes the final report for work performed during the period January 1, 1990 - June 30, 1992.

The Device Models portion of the investigation centers on the development of computer models which can be used to predict the local electromagnetic fields for various power system components or devices, including various transmission line configurations. This work was summarized in previous interim reports. More recently, there has been interest in the $v \times B$ voltage drop developed along the length of the space station structure as a result of the motion at velocity v through the earth's magnetic B field. This voltage difference along the structure results in a current in the conducting plasma surrounding the space station. An analysis of the $v \times B$ effect, including plots of the current density distribution for a cylindrical model of the space station, are summarized in Section 2 of this report.

The Radiation Sources portion of the investigation centers on the development of computer models to simulate the propagation of electromagnetic waves in the ionospheric plasma and the radiation from antennas simulating EMI sources on the space station. This work is summarized in Section 3 of this report.

1

2. Device Models

1 Introduction

An electrodynamic system of the space station freedom in the earth's geomagnetic field in the ionosphere is shown in Fig.2.1. A cylinder type space station is moving at a speed, $\overline{V}_s$, on its orbit surrounding the earth in the geomagnetic field, $\overline{B}_g$. The motion of the space station through the geomagnetic field results in an electromotive force (emf), $\overline{V}_s \times \overline{B}_g$, along its length and causes potential drop across the space station. Because the plasma ionosphere environment surrounding the space station is conductive, a current between the space station and the plasma is induced. This work presents the governing differential equations of this $\overline{V}_s \times \overline{B}_g$ problem, the formulation of the 3D finite element (3D-FE) model for this problem, with the electric scalar potential (ESP) as the field variable, and the consequent computation of the induced current distribution. Due to the infinite boundary of this problem, the absorbing boundary condition (ABC) method is mentioned as one possible future work, for dealing with this type of open boundary problems.

2 Derivation of Governing Equations

For the problem described in the previous section, the total region can be divided into two subregions, Ω_1, and Ω_2 (See Fig.2.2). Region, Ω_1, represents the structure of the space station and is moving at a speed, $\overline{V}_s$, in the geomagnetic field, $\overline{B}_g$. In region, Ω_2, the conductivity $\overline{\overline{\sigma}}_2$ equivalent to the plasma environment may be anisotropic. Surface, S, is the interface boundary between region, Ω_1, and region, Ω_2, on which some electric field and current density continuity conditions should be satisfied. Since the potentials will tend to zero while the boundary, Γ, is extending to infinity, the asymptotic (or absorbing) boundary conditions (ABCs) can be applied on the outer boundary, Γ.

In region, Ω_1:

Because of the $\overline{V} \times \overline{B}$ component, there are two kinds of electric fields in the region Ω_1: an induced electric field, $\overline{E}_i$, and an external electric field, $\overline{E}_e$. The induced field, $\overline{E}_i$, can be expressed as follows:

$$\overline{E}_i = \overline{V}_s \times \overline{B}_g \tag{1}$$

The external field, $\overline{E}_e$, is a conservative field, so that it can be defined as follows:

$$\overline{E}_e = -\nabla \phi_1 \tag{2}$$

where, ϕ_1 is an electric scalar potential (ESP) function in region, Ω_1. The total resultant electric field, $\overline{E}_1$, is the superposition of these two fields, that is:

$$\overline{E}_1 = \overline{E}_i + \overline{E}_e = \overline{V}_s \times \overline{B}_g - \nabla \phi_1 \tag{3}$$

The current density, $\overline{J}_1$, is proportional to the total electric field intensity, $\overline{E}_1$, hence

$$\overline{J}_1 = \sigma_1 \overline{E}_1 = \sigma_1(\overline{E}_i + \overline{E}_e) = -\sigma_1(\nabla \phi_1 - (\overline{V}_s \times \overline{B}_g)) \tag{4}$$

where, σ_1 is the conductivity of region, Ω_1, which is homogeneous. The following current continuity condition must be satisfied anywhere:

$$\nabla \cdot \overline{J}_1 = 0 \tag{5}$$

Substituting (4) into (5), one obtains:

$$\nabla \cdot [\sigma_1(\nabla \phi_1 - (\overline{V}_s \times \overline{B}_g))] = 0 \tag{6}$$

Because both σ_1 and $(\overline{V}_s \times \overline{B}_g)$ are constant, $\nabla \cdot [\sigma_1(\overline{V}_s \times \overline{B}_g)] = 0$, equation (6) can be rewritten as follows:

$$\nabla \cdot [\sigma_1(\nabla \phi_1)] = 0 \qquad in\ \Omega_1 \tag{7}$$

In region, Ω_2:

Only an external field exists. It can be defined as follows:

$$\overline{E}_2 = -\nabla \phi_2 \tag{8}$$

where, ϕ_2 is an electric scalar potential function in region, Ω_2. The current density, $\overline{J}_2$, in region, Ω_2, can be written as follows:

$$\overline{J}_2 = \overline{\overline{\sigma}}_2 \overline{E}_2 \tag{9}$$

where, $\overline{\overline{\sigma}}_2$ is the conductivity matrix of region, Ω_2, resulting from the possible anisotropic properties of this region. Using the current continuity condition again, one obtains:

$$\nabla \cdot \overline{J}_2 = 0 \tag{10}$$

3

Substituting (9) into (10) gives:

$$\nabla \cdot [\overline{\overline{\sigma}}_2 \overline{E}_2] = 0 \tag{11}$$

Meanwhile, substituting (8) into (11) yields the following:

$$\nabla \cdot [\overline{\overline{\sigma}}_2 (\nabla \phi_2)] = 0 \qquad in \ \Omega_2 \tag{12}$$

On boundary, S:

From electromagnetic field theory, on the boundary, S, the tangential component of the electric field should be continuous and the normal component of the current density should also be continuous. These two continuity conditions can be written as follows:

$$\oint \overline{E} \cdot \vec{dl} = 0 \rightarrow (\overline{E}_2 - \overline{E}_1)_t = 0 \rightarrow [-\nabla \phi_2 + \nabla \phi_1 - \overline{V}_s \times \overline{B}_g]_t = 0 \tag{13}$$

$$\oint \overline{J} \cdot \vec{ds} = 0 \rightarrow (\overline{J}_2 - \overline{J}_1)_n = 0 \rightarrow [-\overline{\overline{\sigma}}_2 \nabla \phi_2 - \sigma_1(-\nabla \phi_1 + \overline{V}_s \times \overline{B}_g)]_n = 0 \tag{14}$$

where, the subscripts, n and t denote the normal direction and tangential direction on boundary, S, respectively.

On boundary, Γ:

An m-th order asymptotic boundary condition [1] can be assumed to be satisfied on the boundary, Γ. This can be expressed as follows:

$$B_m \phi_2 = 0 \tag{15}$$

where, B_m is the $m-$th order differential operator.

Governing Equations:

In summary, the governing equations for the $(\overline{V}_s \times \overline{B}_g)$ problem with boundary coupling conditions and asymptotic boundary conditions are as follows:

$$\nabla \cdot [\sigma_1(\nabla \phi_1)] = 0 \qquad in \ \Omega_1 \tag{16}$$

$$\nabla \cdot [\overline{\overline{\sigma}}_2(\nabla \phi_2)] = 0 \qquad in \ \Omega_2 \tag{17}$$

$$(\nabla \phi_1 - \nabla \phi_2)_t = (\overline{V}_s \times \overline{B}_g)_t \qquad on \ S \tag{18}$$

$$[\sigma_1(\nabla \phi_1) - \overline{\overline{\sigma}}_2(\nabla \phi_2)]_n = \sigma_1(\overline{V}_s \times \overline{B}_g)_n \qquad on \ S \tag{19}$$

and

$$B_m \phi_2 = 0 \qquad on \ \Gamma \tag{20}$$

3 Finite Element Formulation

Using the Galerkin-Weighted Residual (GWR) method [2], one can obtain the integral equations equivalent to the differential equations which were derived in the previous section, equations (16) through (20). The integral equations can be discretized by finite element methods [2].

3.1 The Galerkin-Weighted Residual (GWR) method

Using the GWR method, the integral equations can be obtained from the partial differential equations (16) and (17) as follows:

$$\int_{\Omega_1} W \nabla \cdot (\sigma_1(\nabla \phi_1)) d\Omega = 0 \tag{21}$$

$$\int_{\Omega_2} W \nabla \cdot (\overline{\overline{\sigma}}_2(\nabla \phi_2)) d\Omega = 0 \tag{22}$$

where, W is an arbitrary scalar weight function.

From vector calculus, one can write a vector identity as follows:

$$\nabla \cdot (f\overline{F}) = f \nabla \cdot \overline{F} + \nabla f \cdot \overline{F} \Longrightarrow f \nabla \cdot \overline{F} = \nabla \cdot (f\overline{F}) - \nabla f \cdot \overline{F} \tag{23}$$

where, f is any scalar function and $\overline{F}$ is any vector function. Let $\overline{F} = \sigma\nabla\phi$, and $f = W$, one can obtain the following useful transformation from (23):

$$W\nabla \cdot (\sigma\nabla\phi) = \nabla \cdot (W(\sigma\nabla\phi)) - (\nabla W) \cdot (\sigma\nabla\phi) \tag{24}$$

Using the relationship shown in (24), one can rewrite (21) and (22) as follows:

$$\int_{\Omega_1} W\nabla \cdot (\sigma_1(\nabla\phi_1))d\Omega = \int_{\Omega_1} \nabla \cdot (W(\sigma_1\nabla\phi_1))d\Omega - \int_{\Omega_1} (\nabla W) \cdot (\sigma_1\nabla\phi_1)d\Omega = 0 \tag{25}$$

$$\int_{\Omega_2} W\nabla \cdot (\overline{\overline{\sigma}}_2(\nabla\phi_2))d\Omega = \int_{\Omega_2} \nabla \cdot (W(\overline{\overline{\sigma}}_2\nabla\phi_2))d\Omega - \int_{\Omega_2} (\nabla W) \cdot (\overline{\overline{\sigma}}_2\nabla\phi_2)d\Omega = 0 \tag{26}$$

From vector calculus , Gauss' theorem gives:

$$\int_{\Omega} \nabla \cdot \overline{F}d\Omega = \oint_S \overline{F} \cdot d\overline{s} \tag{27}$$

where, Ω is a space volume, the closed surface of which is S. The normal direction $\overline{s}$ is out of the volume.

Applying Gauss' theorem, equation (27), to (25) and (26), one can obtain the following:

$$-\int_{\Omega_1} (\nabla W) \cdot (\sigma_1\nabla\phi_1)d\Omega + \oint_{S_1} W(\sigma_1\nabla\phi_1) \cdot d\overline{s} = 0 \tag{28}$$

$$\oint_{S_2} W(\overline{\overline{\sigma}}_2\nabla\phi_2) \cdot d\overline{s} + \oint_{\Gamma} W(\overline{\overline{\sigma}}_2\nabla\phi_2) \cdot d\overline{s} - \int_{\Omega_2} (\nabla W) \cdot (\overline{\overline{\sigma}}_2\nabla\phi_2)d\Omega = 0 \tag{29}$$

where, $S_1 = -S_2$. The second term of the left side in (29) can be dealt with the asymptotic boundary condition (ABC) method which will be discussed in future work and here assumed to be zero (the nature boundary condition). That is:

$$\oint_{\Gamma} W(\overline{\overline{\sigma}}_2\nabla\phi_2) \cdot d\overline{s} = 0 \tag{30}$$

Therefore one can merge equations (28) and (29) into the following:

$$\int_{\Omega_1} (\nabla W) \cdot (\sigma_1\nabla\phi_1)d\Omega + \int_{\Omega_2} (\nabla W) \cdot (\overline{\overline{\sigma}}_2\nabla\phi_2)d\Omega = \oint_{S_1} W[\sigma_1(\nabla\phi_1) - \overline{\overline{\sigma}}_2(\nabla\phi_2)]_n ds \tag{31}$$

6

Substituting the boundary condition (19) into (31) yields:

$$\int_{\Omega_1} (\nabla W) \cdot (\sigma_1 \nabla \phi_1) d\Omega + \int_{\Omega_2} (\nabla W) \cdot (\overline{\overline{\sigma}}_2 \nabla \phi_2) d\Omega = \oint_{S_1} W \sigma_1 (\overline{V}_s \times \overline{B}_g)_n ds \tag{32}$$

To simplifying the problem, one introduces some definitions as follows:

$$\underline{\sigma}|_{\Omega_1} = \sigma_1; \qquad \underline{\sigma}|_{\Omega_2} = \overline{\overline{\sigma}}_2; \tag{33}$$

and

$$\phi|_{\Omega_1} = \phi_1; \qquad \phi|_{\Omega_2} = \phi_2 \tag{34}$$

Using the above definitions, one can rewrite equation (32) as follows:

$$\int_{\Omega = \Omega_1 \cup \Omega_2} (\nabla W) \cdot (\underline{\sigma} \nabla \phi) d\Omega = \oint_{S_1} W \underline{\sigma} (\overline{V}_s \times \overline{B}_g)_n ds \tag{35}$$

3.2   Discretization by FE Method

Define an interpolation function of the scalar potential in a finite element which has m nodes as follows:

$$\phi^e = \sum_{j=l_1}^{l_m} N_j \phi_j \tag{36}$$

where, N_j is a shape function, and ϕ_j is the potential value at node j. The node numbers of a given element are $l_1, l_2, \cdots, l_m$.

Let us define the weight function in (35) as follows:

$$W = N_i \qquad i = l_1, l_2, \cdots, l_m \tag{37}$$

Applying (36) and (37) to (35), one can obtain the element integral function as follows:

$$\int_{\Omega^e} (\nabla N_i) \underline{\sigma} (\sum_{j=l_1}^{l_m} \nabla N_j \phi_j) d\Omega = \oint_{S_1^e} N_i \underline{\sigma} (\overline{V}_s \times \overline{B}_g)_n ds \tag{38}$$

$$i = l_1, l_2, \cdots, l_m$$

7

Moving the summation out of the integral, one can rewrite the previous equation as follows:

$$\sum_{j=l_1}^{l_m} [\int_{\Omega^e} (\nabla N_i \underline{\sigma} \nabla N_j) d\Omega] \phi_j = \oint_{S_1^e} N_i \underline{\sigma} (\overline{V}_s \times \overline{B}_g)_n ds \qquad (39)$$
$$i, = l_1, l_2, \cdots, l_m$$

This relationship can be written in the matrix form as follows:

$$\begin{bmatrix} s_{l_1,l1} & s_{l_1,l2} & \cdots & s_{l_1,lm} \\ \vdots & \vdots & \vdots & \vdots \\ \vdots & \vdots & \vdots & \vdots \\ s_{l_m,l1} & s_{l_m,l2} & \cdots & s_{l_m,lm} \end{bmatrix} \begin{bmatrix} \phi_{l_1} \\ \vdots \\ \vdots \\ \phi_{l_m} \end{bmatrix} = \begin{bmatrix} b_{l_1} \\ \vdots \\ \vdots \\ b_{l_m} \end{bmatrix} \qquad (40)$$

Hence, the elemental FE equation can be expressed as follows:

$$\underline{S}^e \cdot \underline{\phi}^e = \underline{b}^e \qquad (41)$$

where,

$$s_{ij} = \int_{\Omega^e} (\nabla N_i \underline{\sigma} \nabla N_j) d\Omega$$
$$b_i = \oint_{S_1^e} N_i \underline{\sigma} (\overline{V}_s \times \overline{B}_g)_n ds \qquad (42)$$
$$i, j = l_1, l_2, \cdots, l_m$$

and

$$\phi^e = [\phi_{l_1}, \phi_{l_2}, \cdots, \phi_{l_m}]^t \qquad (43)$$

The tangential continuity condition on the interface, S, $(\nabla \phi_1 - \nabla \phi_2)_t = (\overline{V}_s \times \overline{B}_g)_t$, can be considered as a potential jump distribution by which the previous FE formulations should be modified. In the next section, the potential jump distribution will be discussed.

3.3   FE Formulations Modified by Potential Jump Distribution

On surface, S, we define the potentials as follows:

$$\phi|_S = \phi_2; \qquad (\phi_2 - \phi_1)|_S = T \qquad (44)$$

Consider an element, e, which belongs to region, Ω_1, and on interface, S. The total m nodes on element, e, are $l_1, l_2, \cdots, l_{m-n}, l'_1, l'_2, \cdots, l'_n$, in which $l'_1, l'_2, \cdots, l'_n$ are on the interface,

8

S_e. Meanwhile, the interpolation function in such kind of elements can be expressed as follows:

$$\phi_1^e = \sum_{j=l_1}^{l_{m-n}} N_j \phi_{1j} + \sum_{j=l_1'}^{l_n'} N_j \phi_{1j} \tag{45}$$

Because of the fact that $\phi_1 = \phi_2 - T$ on nodes $l_1', l_2', \cdots, l_n'$, the previous equation can be expressed as follows:

$$\phi_1^e = \sum_{j=l_1}^{l_{m-n}} N_j \phi_{1j} + \sum_{j=l_1'}^{l_n'} N_j(\phi_{2j} - T_j) = \{ \sum_{j=l_1}^{l_{m-n}} N_j \phi_{1j} + \sum_{j=l_1'}^{l_n'} N_j \phi_{2j} \} - \sum_{j=l_1'}^{l_n'} N_j T_j \tag{46}$$

Applying the definition of the potentials in (34) and (44), one can rewrite the previous equation as follows:

$$\phi^e = \sum_{j=l_1}^{l_m} N_j \phi_j - \sum_{j=l_1'}^{l_n'} N_j T_j \tag{47}$$

$$\nabla \phi^e = \sum_{j=l_1}^{l_m} \nabla N_j \phi_j - \sum_{j=l_1'}^{l_n'} \nabla N_j T_j \tag{48}$$

For an element which belongs to region, Ω_1, and on surface, S, one can obtain the elemental equation as follows:

$$\sum_{j=l_1}^{l_m} [\int_{\Omega^e} (\nabla N_i \underline{\sigma} \nabla N_j) d\Omega] \phi_j - \sum_{j=l_1'}^{l_n'} [\int_{\Omega_1^e} (\nabla N_i \underline{\sigma} \nabla N_j) d\Omega] T_j = \oint_{S_1^e} N_i \underline{\sigma} (\overline{V}_s \times \overline{B}_g)_n ds \tag{49}$$

$$i = l_1, l_2, \cdots, l_m$$

or

$$\sum_{j=l_1}^{l_m} [\int_{\Omega^e} (\nabla N_i \underline{\sigma} \nabla N_j) d\Omega] \phi_j = \oint_{S_1^e} N_i \underline{\sigma} (\overline{V}_s \times \overline{B}_g)_n ds + \sum_{j=l_1'}^{l_n'} [\int_{\Omega_1^e} (\nabla N_i \underline{\sigma} \nabla N_j) d\Omega] T_j \tag{50}$$

$$i = l_1, l_2, \cdots, l_m$$

Rewriting the modified FE elemental equations in matrix form one obtains the following:

$$\begin{bmatrix} s_{l_1,l1} & s_{l_1,l2} & \cdots & s_{l_1,lm} \\ \vdots & \vdots & \vdots & \vdots \\ \vdots & \vdots & \vdots & \vdots \\ s_{l_m,l1} & s_{l_m,l2} & \cdots & s_{l_m,lm} \end{bmatrix} \begin{bmatrix} \phi_{l_1} \\ \vdots \\ \vdots \\ \phi_{l_m} \end{bmatrix} = \begin{bmatrix} b_{l_1} \\ \vdots \\ \vdots \\ b_{l_m} \end{bmatrix} \tag{51}$$

where,

$$s_{ij} = \int_{\Omega^e} (\nabla N_i \underline{\sigma} \nabla N_j) d\Omega \qquad\qquad i, j = l_1, l_2, \cdots, l_m$$

$$b_i = \oint_{S_1^e} N_i \underline{\sigma} (\overline{V}_s \times \overline{B}_g)_n ds + \sum_{j=l_1'}^{l_n'} s_{ij} T_j \quad i = l_1, l_2, \cdots, l_m, \qquad j = l_1', l_2', \cdots, l_n', \qquad (52)$$

The computation of the potential jump distribution, T, will be presented in the next section.

4 Computation of the Potential Jump Distribution

4.1 Surface Element Analysis

From equation (18), one can see that the potential jump distribution on surface, S, is governed by the following differential equation:

$$\nabla T = -(\overline{V}_s \times \overline{B}_g)_t = -\overline{E}_{vt} \qquad\qquad (53)$$

where, $T = (\phi_2 - \phi_1)|_S$

One can choose a cost functional to be minimized on boundary, S, as follows:

$$F(T) = \int_S |\nabla T + \overline{E}_{vt}|^2 ds = \sum_{e=1}^{NE_s} \int_{S^e} |\nabla T + \overline{E}_{vt}|^2 ds \qquad\qquad (54)$$

where, NE_s is the total number of the surface elements, and S^e is the area of a given surface element. Here we assume that for every element in region, Ω_1, no more than one element surface is on the surface, S. In this work, first order tetrahedral finite elements are chosen and only nodes, l', m' and n', can be on surface, S, (see Fig.2.3.).

Define an interpolation function on surface S_e as follows:

$$T = N_{l'} T_{l'} + N_{m'} T_{m'} + N_{n'} T_{n'} \qquad\qquad (55)$$

where, $N_{l'}, N_{m'}$ and $N_{n'}$ are shape functions on S_e, and $T_{l'}, T_{m'}$ and $T_{n'}$ are the potential jump distribution on the nodes, l', m' and n'.

A local coordinate system (u, v, w) should be adopted (see Fig.2.3.).

$$T = T(u, v) = N_{l'}(u, v) T_{l'} + N_{m'}(u, v) T_{m'} + N_{n'}(u, v) T_{n'} \qquad\qquad (56)$$

10

Here,

$$\frac{\partial T}{\partial u} = \frac{\partial N_{l'}}{\partial u}T_{l'} + \frac{\partial N_{m'}}{\partial u}T_{m'} + \frac{\partial N_{n'}}{\partial u}T_{n'} \tag{57}$$

$$\frac{\partial T}{\partial v} = \frac{\partial N_{l'}}{\partial v}T_{l'} + \frac{\partial N_{m'}}{\partial v}T_{m'} + \frac{\partial N_{n'}}{\partial v}T_{n'} \tag{58}$$

$$\overline{E}_{vt} = E_u \hat{a}_u + E_v \hat{a}_v \tag{59}$$

where, E_u and E_v are constant.

$$\nabla T = \frac{\partial T}{\partial u}\hat{a}_u + \frac{\partial T}{\partial v}\hat{a}_v \tag{60}$$

Substituting (59) and (60) into the cost functional, (54), gives:

$$
\begin{aligned}
F(T) &= \sum_{e=1}^{NE_s} \int_{S^e} |(\frac{\partial T}{\partial u}\hat{a}_u + \frac{\partial T}{\partial v}\hat{a}_v) + (E_u\hat{a}_u + E_v\hat{a}_v)|^2 dudv \\
&= \sum_{e=1}^{NE_s} \int_{S^e} |(\frac{\partial T}{\partial u} + E_u)\hat{a}_u + (\frac{\partial T}{\partial v} + E_v)\hat{a}_v|^2 dudv \\
&= \sum_{e=1}^{NE_s} \int_{S^e} [(\frac{\partial T}{\partial u} + E_u)^2 + (\frac{\partial T}{\partial v} + E_v)^2] dudv
\end{aligned}
\tag{61}
$$

The minimization of the cost functional is as follows:

$$
\begin{aligned}
\frac{\partial F(T)}{\partial T_i} &= \frac{\partial}{\partial T_i}\{\sum_{e=1}^{NE_s} \int_{S^e} [(\frac{\partial T}{\partial u} + E_u)^2 + (\frac{\partial T}{\partial v} + E_v)^2] dudv \\
&= \sum_{e=1}^{NE_s} 2\int_{S^e} [(\frac{\partial T}{\partial u} + E_u)\frac{\partial}{\partial T_i}(\frac{\partial T}{\partial u}) + (\frac{\partial T}{\partial v} + E_v)\frac{\partial}{\partial T_i}(\frac{\partial T}{\partial v})] dudv \\
&= \sum_{e=1}^{NE_s} 2\int_{S^e} [(\frac{\partial T}{\partial u} + E_u)(\frac{\partial N_i}{\partial u}) + (\frac{\partial T}{\partial v} + E_v)(\frac{\partial N_i}{\partial v})] dudv \\
&= 0
\end{aligned}
\tag{62}
$$

where, $i = l', m', n'$.

Substituting (57) and (58) into (62) yields the following:

$$
\begin{aligned}
\frac{\partial F(T)}{\partial T_i} &= \sum_{e=1}^{NE_s} 2\int_{S^e} [(\frac{\partial N_{l'}}{\partial u}T_{l'} + \frac{\partial N_{m'}}{\partial u}T_{m'} + \frac{\partial N_{n'}}{\partial u}T_{n'} + E_u)(\frac{\partial N_i}{\partial u}) \\
&\quad + (\frac{\partial N_{l'}}{\partial v}T_{l'} + \frac{\partial N_{m'}}{\partial v}T_{m'} + \frac{\partial N_{n'}}{\partial v}T_{n'} + E_v)(\frac{\partial N_i}{\partial u})] dudv \\
&= \sum_{e=1}^{NE_s} 2\int_{S^e} [(\frac{\partial N_i}{\partial u}\frac{\partial N_{l'}}{\partial u} + \frac{\partial N_i}{\partial v}\frac{\partial N_{l'}}{\partial v})T_{l'} + (\frac{\partial N_i}{\partial u}\frac{\partial N_{m'}}{\partial u} + \frac{\partial N_i}{\partial v}\frac{\partial N_{m'}}{\partial v})T_{m'} \\
&\quad + (\frac{\partial N_i}{\partial u}\frac{\partial N_{n'}}{\partial u} + \frac{\partial N_i}{\partial v}\frac{\partial N_{n'}}{\partial v})T_{n'} + \frac{\partial N_i}{\partial u}E_u + \frac{\partial N_i}{\partial v}E_v] dudv = 0
\end{aligned}
\tag{63}
$$

where $i = l', m', n'$

In the previous equation, all partial derivative terms are constant because of the nature of the interpolation polynomials in first order elements, so that the elemental equation can be expressed on S^e as follows:

$$\Delta(\frac{\partial N_i}{\partial u}\frac{\partial N_{l'}}{\partial u} + \frac{\partial N_i}{\partial v}\frac{\partial N_{l'}}{\partial v})T_{l'} + \Delta(\frac{\partial N_i}{\partial u}\frac{\partial N_{m'}}{\partial u} + \frac{\partial N_i}{\partial v}\frac{\partial N_{m'}}{\partial v})T_{m'}$$
$$+\Delta(\frac{\partial N_i}{\partial u}\frac{\partial N_{n'}}{\partial u} + \frac{\partial N_i}{\partial v}\frac{\partial N_{n'}}{\partial v})T_{n'} = -\Delta(\frac{\partial N_i}{\partial u}E_u + \frac{\partial N_i}{\partial v}E_v) \tag{64}$$

$$i = l', m', n'$$

where, Δ is the area of the triangular element, e.

The previous equation can be expressed in matrix form as follows:

$$\begin{bmatrix} k_{l'l'} & k_{l'm'} & k_{l'n'} \\ k_{m'l'} & k_{m'm'} & k_{m'n'} \\ k_{n'l'} & k_{n'm'} & k_{n'n'} \end{bmatrix} \begin{bmatrix} T_{l'} \\ T_{m'} \\ T_{n'} \end{bmatrix} = \begin{bmatrix} C_{l'} \\ C_{m'} \\ C_{n'} \end{bmatrix} \tag{65}$$

where,

$$\begin{aligned} k_{ij} &= \Delta(\frac{\partial N_i}{\partial u}\frac{\partial N_j}{\partial u} + \frac{\partial N_i}{\partial v}\frac{\partial N_j}{\partial v}) \\ C_i &= -\Delta(\frac{\partial N_i}{\partial u}E_u + \frac{\partial N_i}{\partial v}E_v) \\ i,j &= l', m', n' \end{aligned} \tag{66}$$

4.2 Local Coordinate System

The local coordinate system $(\hat{a}_u, \hat{a}_v, \hat{a}_w)$, see Fig.2.3, can be calculated as follows:

$$\hat{a}_u = u_x\hat{a}_x + u_y\hat{a}_y + u_z\hat{a}_z = \frac{\overline{l'm'}}{|\overline{l'm'}|} = \frac{x_{m'l'}}{L_{m'l'}}\hat{a}_x + \frac{y_{m'l'}}{L_{m'l'}}\hat{a}_y + \frac{z_{m'l'}}{L_{m'l'}}\hat{a}_z \tag{67}$$

or,

$$\hat{a}_u = \begin{bmatrix} u_x \\ u_y \\ u_z \end{bmatrix} = \frac{1}{L_{m'l'}} \begin{bmatrix} x_{m'l'} \\ y_{m'l'} \\ z_{m'l'} \end{bmatrix} \tag{68}$$

where $\begin{bmatrix} x_{m'l'} \\ y_{m'l'} \\ z_{m'l'} \end{bmatrix} = \begin{bmatrix} x_{m'} - x_{l'} \\ y_{m'} - y_{l'} \\ z_{m'} - z_{l'} \end{bmatrix}$ and $L_{m'l'} = \sqrt{x_{m'l'}^2 + y_{m'l'}^2 + z_{m'l'}^2}$.

$$\hat{a}_w = w_x\hat{a}_x + w_y\hat{a}_y + w_z\hat{a}_z = \frac{(\overline{l'm'} \times \overline{l'n'})}{|\overline{l'm'} \times \overline{l'n'}|} = \frac{1}{2\Delta} \begin{vmatrix} \hat{a}_x & \hat{a}_y & \hat{a}_z \\ x_{m'l'} & y_{m'l'} & z_{m'l'} \\ x_{n'l'} & y_{n'l'} & z_{n'l'} \end{vmatrix} \tag{69}$$

12

or,

$$\hat{a}_w = \begin{bmatrix} w_x \\ w_y \\ w_z \end{bmatrix} = \frac{1}{2\Delta} \begin{bmatrix} y_{m'l'}z_{n'l'} - y_{n'l'}z_{m'l'} \\ x_{n'l'}z_{m'l'} - x_{m'l'}z_{n'l'} \\ x_{m'l'}y_{n'l'} - x_{n'l'}y_{m'l'} \end{bmatrix} \tag{70}$$

where, $\begin{bmatrix} x_{n'l'} \\ y_{n'l'} \\ z_{n'l'} \end{bmatrix} = \begin{bmatrix} x_{n'} - x_{l'} \\ y_{n'} - y_{l'} \\ z_{n'} - z_{l'} \end{bmatrix}$ and Δ is the area of the triangle $l'm'n'$ on surface S^e:

$$2\Delta = \sqrt{(y_{m'l'}z_{n'l'} - y_{n'l'}z_{m'l'})^2 + (x_{n'l'}z_{m'l'} - x_{m'l'}z_{n'l'})^2 + (x_{m'l'}y_{n'l'} - x_{n'l'}y_{m'l'})^2} \tag{71}$$

$$\begin{aligned} \hat{a}_v &= v_x\hat{a}_x + v_y\hat{a}_y + v_z\hat{a}_z = \hat{a}_w \times \hat{a}_u \\ &= \frac{1}{2\Delta L_{m'l'}} \begin{vmatrix} \hat{a}_x & \hat{a}_y & \hat{a}_z \\ y_{m'l'}z_{n'l'} - y_{n'l'}z_{m'l'} & x_{n'l'}z_{m'l'} - x_{m'l'}z_{n'l'} & x_{m'l'}y_{n'l'} - x_{n'l'}y_{m'l'} \\ x_{m'l'} & y_{m'l'} & z_{m'l'} \end{vmatrix} \end{aligned} \tag{72}$$

or,

$$\hat{a}_v = \begin{bmatrix} v_x \\ v_y \\ v_z \end{bmatrix} = \frac{1}{2\Delta L_{m'l'}} \begin{bmatrix} (x_{n'l'}z_{m'l'} - x_{m'l'}z_{n'l'})z_{m'l'} - (x_{m'l'}y_{n'l'} - x_{n'l'}y_{m'l'})y_{m'l'} \\ (x_{m'l'}y_{n'l'} - x_{n'l'}y_{m'l'})x_{m'l'} - (y_{m'l'}z_{n'l'} - y_{n'l'}z_{m'l'})z_{m'l'} \\ (y_{m'l'}z_{n'l'} - y_{n'l'}z_{m'l'})y_{m'l'} - (x_{n'l'}z_{m'l'} - x_{m'l'}z_{n'l'})x_{m'l'} \end{bmatrix} \tag{73}$$

4.3 Transformation from Global to Local Coordinates

In the global system, the surface elements are three dimensional but in the local system, they are two dimensional. We need a transformation from the global system to the local system. Assuming node l' is located on the origin point in the local coordinate, one can obtain the nodal transformation as follows:

$$\begin{bmatrix} u_i \\ v_i \end{bmatrix} = \begin{bmatrix} u_x & u_y & u_z \\ v_x & v_y & v_z \end{bmatrix} \begin{bmatrix} x_i - x_{l'} \\ y_i - y_{l'} \\ z_i - z_{l'} \end{bmatrix} \qquad i = l', m', n' \tag{74}$$

The tangential component of $(\overline{V}_s \times \overline{B}_g)$ on the surface, S_e, can be expressed as follows:

$$E_u = \overline{E}_{vt} \cdot \hat{a}_u \tag{75}$$
$$E_v = \overline{E}_{vt} \cdot \hat{a}_v \tag{76}$$

In the local coordinate system, the shape functions become two-dimensional, hence [3]:

$$\begin{aligned} N_{l'} &= \frac{1}{2\Delta}(p_{l'} + q_{l'}u + r_{l'}v) \\ N_{m'} &= \frac{1}{2\Delta}(p_{m'} + q_{m'}u + r_{m'}v) \\ N_{n'} &= \frac{1}{2\Delta}(p_{n'} + q_{n'}u + r_{n'}v) \end{aligned} \tag{77}$$

and

$$
\begin{aligned}
\frac{\partial N_{l'}}{\partial y} &= \frac{q_{l'}}{2\Delta}; & \frac{\partial N_{l'}}{\partial v} &= \frac{r_{l'}}{2\Delta}; \\
\frac{\partial N_{m'}}{\partial u} &= \frac{q_{m'}}{2\Delta}; & \frac{\partial N_{m'}}{\partial v} &= \frac{r_{m'}}{2\Delta}; \\
\frac{\partial N_{n'}}{\partial u} &= \frac{q_{n'}}{2\Delta}; & \frac{\partial N_{n'}}{\partial v} &= \frac{r_{n'}}{2\Delta}
\end{aligned}
\tag{78}
$$

where

$$
\begin{aligned}
p_{l'} &= u_{m'}v_{n'} - u_{n'}v_{m'}; & q_{l'} &= v_{m'} - v_{n'}; r_{l'} = u_{n'} - u_{m'} \\
p_{m'} &= u_{n'}v_{l'} - u_{l'}v_{n'}; & q_{m'} &= v_{n'} - v_{l'}; r_{m'} = u_{l'} - u_{n'} \\
p_{n'} &= u_{l'}v_{m'} - u_{m'}v_{l'}; & q_{n'} &= v_{l'} - v_{m'}; r_{n'} = u_{m'} - u_{l'}
\end{aligned}
\tag{79}
$$

Substituting (78) into (66), one obtains the following:

$$
\begin{bmatrix}
k_{l'l'} & k_{l'm'} & k_{l'n'} \\
k_{m'l'} & k_{m'm'} & k_{m'n'} \\
k_{n'l'} & k_{n'm'} & k_{n'n'}
\end{bmatrix}
\begin{bmatrix}
T_{l'} \\
T_{m'} \\
T_{n'}
\end{bmatrix}
=
\begin{bmatrix}
C_{l'} \\
C_{m'} \\
C_{n'}
\end{bmatrix}
\tag{80}
$$

where,

$$
\begin{aligned}
k_{ij} &= \frac{1}{2\Delta}(q_i q_j + r_i r_j) \\
C_i &= -q_i E_u - r_i E_v \\
i, j &= l', m', n'
\end{aligned}
\tag{81}
$$

5 FE Formulation Using First-Order Tetrahedral Elements

5.1 Shape Function

Fig.2.4. shows a first order tetrahedral finite element by which we can construct an interpolation function as follows:

$$
\begin{cases}
\phi(x, y, z) = \alpha_1 + \alpha_2 x + \alpha_3 y + \alpha_4 z \\
\phi(x_i, y_i, z_i) = \phi_i & i = l, m, n, s
\end{cases}
\tag{82}
$$

On nodes, l, m, n, s, the interpolation functions are as follows:

$$
\begin{aligned}
\alpha_1 &+ \alpha_2 x_l &+ \alpha_3 y_l &+ \alpha_4 z_l &= \phi_l \\
\alpha_1 &+ \alpha_2 x_m &+ \alpha_3 y_m &+ \alpha_4 z_m &= \phi_m \\
\alpha_1 &+ \alpha_2 x_n &+ \alpha_3 y_n &+ \alpha_4 z_n &= \phi_n \\
\alpha_1 &+ \alpha_2 x_s &+ \alpha_3 y_s &+ \alpha_4 z_s &= \phi_s
\end{aligned}
\tag{83}
$$

14

or, in matrix form:

$$\begin{bmatrix} 1 & x_l & y_l & z_l \\ 1 & x_m & y_m & z_m \\ 1 & x_n & y_n & z_n \\ 1 & x_s & y_s & z_s \end{bmatrix} \begin{bmatrix} \alpha_1 \\ \alpha_2 \\ \alpha_3 \\ \alpha_4 \end{bmatrix} = \begin{bmatrix} \phi_l \\ \phi_m \\ \phi_n \\ \phi_s \end{bmatrix} \tag{84}$$

The interpolation coefficients, $\alpha_1, \alpha_2, \alpha_3$ and α_4, can be solved for as follows:

$$\begin{bmatrix} \alpha_1 \\ \alpha_2 \\ \alpha_3 \\ \alpha_4 \end{bmatrix} = \begin{bmatrix} 1 & x_l & y_l & z_l \\ 1 & x_m & y_m & z_m \\ 1 & x_n & y_n & z_n \\ 1 & x_s & y_s & z_s \end{bmatrix}^{-1} \begin{bmatrix} \phi_l \\ \phi_m \\ \phi_n \\ \phi_s \end{bmatrix} = \begin{bmatrix} a_l & a_m & a_n & a_s \\ b_l & b_m & b_n & b_s \\ c_l & c_m & c_n & c_s \\ d_l & d_m & d_n & d_s \end{bmatrix} \begin{bmatrix} \phi_l \\ \phi_m \\ \phi_n \\ \phi_s \end{bmatrix} \tag{85}$$

where,

$$\begin{bmatrix} a_l & a_m & a_n & a_s \\ b_l & b_m & b_n & b_s \\ c_l & c_m & c_n & c_s \\ d_l & d_m & d_n & d_s \end{bmatrix} = \begin{bmatrix} 1 & x_l & y_l & z_l \\ 1 & x_m & y_m & z_m \\ 1 & x_n & y_n & z_n \\ 1 & x_s & y_s & z_s \end{bmatrix}^{-1}$$

Thus:

$$\begin{aligned} \phi(x,y,z) &= \alpha_1 + \alpha_2 x + \alpha_3 y + \alpha_4 z \\ &= (a_l \phi_l + a_m \phi_m + a_n \phi_n + a_s \phi_s) \\ &\quad + (b_l \phi_l + b_m \phi_m + b_n \phi_n + b_s \phi_s) x \\ &\quad + (c_l \phi_l + c_m \phi_m + c_n \phi_n + c_s \phi_s) y \\ &\quad + (d_l \phi_l + d_m \phi_m + d_n \phi_n + d_s \phi_s) z \end{aligned} \tag{86}$$

or,

$$\begin{aligned} \phi(x,y,z) &= N_l \phi_l + N_m \phi_m + N_n \phi_n + N_s \phi_s \\ &= (a_l + b_l x + c_l y + d_l z) \phi_l \\ &\quad + (a_m + b_m x + c_m y + d_m z) \phi_m \\ &\quad + (a_n + b_n x + c_n y + d_n z) \phi_n \\ &\quad + (a_s + b_s x + c_s y + d_s z) \phi_s \end{aligned} \tag{87}$$

Here, the shape functions are as follows:

$$\begin{cases} N_l = (a_l + b_l x + c_l y + d_l z) \\ N_m = (a_m + b_m x + c_m y + d_m z) \\ N_n = (a_n + b_n x + c_n y + d_n z) \\ N_s = (a_s + b_s x + c_s y + d_s z) \end{cases} \tag{88}$$

where,

$$a_l = \begin{vmatrix} x_m & y_m & z_m \\ x_n & y_n & z_n \\ x_s & y_s & z_s \end{vmatrix} /6V \; ; \qquad a_m = - \begin{vmatrix} x_l & y_l & z_l \\ x_n & y_n & z_n \\ x_s & y_s & z_s \end{vmatrix} /6V \; ;$$

$$a_n = \begin{vmatrix} x_l & y_l & z_l \\ x_m & y_m & z_m \\ x_s & y_s & z_s \end{vmatrix} /6V \; ; \qquad a_s = - \begin{vmatrix} x_l & y_l & z_l \\ x_m & y_m & z_m \\ x_n & y_n & z_n \end{vmatrix} /6V \; ;$$

$$b_l = - \begin{vmatrix} 1 & y_m & z_m \\ 1 & y_n & z_n \\ 1 & y_s & z_s \end{vmatrix} /6V \; ; \qquad b_m = \begin{vmatrix} 1 & y_l & z_l \\ 1 & y_n & z_n \\ 1 & y_s & z_s \end{vmatrix} /6V \; ;$$

$$b_n = - \begin{vmatrix} 1 & y_l & z_l \\ 1 & y_m & z_m \\ 1 & y_s & z_s \end{vmatrix} /6V \; ; \qquad b_s = \begin{vmatrix} 1 & y_l & z_l \\ 1 & y_m & z_m \\ 1 & y_n & z_n \end{vmatrix} /6V \; ;$$

$$c_l = \begin{vmatrix} 1 & x_m & z_m \\ 1 & x_n & z_n \\ 1 & x_s & z_s \end{vmatrix} /6V \; ; \qquad c_m = - \begin{vmatrix} 1 & x_l & z_l \\ 1 & x_n & z_n \\ 1 & x_s & z_s \end{vmatrix} /6V \; ;$$

$$c_n = \begin{vmatrix} 1 & x_l & z_l \\ 1 & x_m & z_m \\ 1 & x_s & z_s \end{vmatrix} /6V \; ; \qquad c_s = - \begin{vmatrix} 1 & x_l & z_l \\ 1 & x_m & z_m \\ 1 & x_n & z_n \end{vmatrix} /6V \; ;$$

$$d_l = - \begin{vmatrix} 1 & x_m & y_m \\ 1 & x_n & y_n \\ 1 & x_s & y_s \end{vmatrix} /6V \; ; \qquad d_m = \begin{vmatrix} 1 & x_l & y_l \\ 1 & x_n & y_n \\ 1 & x_s & y_s \end{vmatrix} /6V \; ;$$

$$d_n = - \begin{vmatrix} 1 & x_l & y_l \\ 1 & x_m & y_m \\ 1 & x_s & y_s \end{vmatrix} /6V \; ; \qquad d_s = \begin{vmatrix} 1 & x_l & y_l \\ 1 & x_m & y_m \\ 1 & x_n & y_n \end{vmatrix} /6V \; ;$$

and,

$$\nabla N_l = \frac{\partial N_l}{\partial x}\hat{a}_x + \frac{\partial N_l}{\partial y}\hat{a}_y + \frac{\partial N_l}{\partial z}\hat{a}_z = (b_l\hat{a}_x + c_l\hat{a}_y + d_l\hat{a}_z) \tag{89}$$

$$\nabla N_m = \frac{\partial N_m}{\partial x}\hat{a}_x + \frac{\partial N_m}{\partial y}\hat{a}_y + \frac{\partial N_m}{\partial z}\hat{a}_z = (b_m\hat{a}_x + c_m\hat{a}_y + d_m\hat{a}_z) \tag{90}$$

$$\nabla N_n = \frac{\partial N_n}{\partial x}\hat{a}_x + \frac{\partial N_n}{\partial y}\hat{a}_y + \frac{\partial N_n}{\partial z}\hat{a}_z = (b_n\hat{a}_x + c_n\hat{a}_y + d_n\hat{a}_z) \tag{91}$$

$$\nabla N_s = \frac{\partial N_s}{\partial x}\hat{a}_x + \frac{\partial N_s}{\partial y}\hat{a}_y + \frac{\partial N_s}{\partial z}\hat{a}_z = (b_s\hat{a}_x + c_s\hat{a}_y + d_s\hat{a}_z) \tag{92}$$

where, $6V = \begin{vmatrix} 1 & x_l & y_l & z_l \\ 1 & x_m & y_m & z_m \\ 1 & x_n & y_n & z_n \\ 1 & x_s & y_s & z_s \end{vmatrix}$

16

5.2 FE Formulation

Using the first order tetrahedral element, one can discretize elemental equation, (52), as follows:

$$
\begin{aligned}
S_{ij} &= \int_{\Omega^e} \{\sigma_x \frac{\partial N_i}{\partial x}\frac{\partial N_j}{\partial x} + \sigma_y \frac{\partial N_i}{\partial y}\frac{\partial N_j}{\partial y} + \sigma_z \frac{\partial N_i}{\partial z}\frac{\partial N_j}{\partial z}\}d\Omega \\
&= (\sigma_x b_i b_j + \sigma_y c_i c_j + \sigma_z d_i d_j) \cdot V \\
b_i &= \sigma_1(\overline{V}_s \times \overline{B}_g)_n \int_{S_1^e} N_i ds + \sum_{j'=l',m',n',s'} S_{i,j'}T_{j'} \\
&= \sigma_1(\overline{V}_s \times \overline{B}_g)_n \frac{\Delta_{lmn}}{3} + \sum_{j'=l',m',n',s'} S_{i,j'}T_{j'} \\
i,j &= l,m,n,s
\end{aligned}
\tag{93}
$$

where, Δ_{lmn} is the area of the triangle (nodes l,m,n); subscript, n denotes the normal direction on surface S_1^e; symbol, j' is the node on surface S_1^e; V is the volume of the tetrahedral element, e.

6 Calculation of Current Density

The current density is proportional to the electric field intensity.

In region, Ω_1:

$$
\overline{J}_1 = \sigma_1 \overline{E}_1 = \sigma_1(\overline{E}_i + \overline{E}_e) = -\sigma_1(\nabla \phi_1 - (\overline{V}_s \times \overline{B}_g))
\tag{94}
$$

where, σ_1 is the conductivity of region, Ω_1, which is homogeneous.

From (47) and (48), the element potential and its gradient can be expressed as follows:

$$
\phi^e = \sum_{j=l_1}^{lm} N_j \phi_j - \sum_{j=l_1'}^{l_n'} N_j T_j
\tag{95}
$$

$$
\nabla \phi^e = \sum_{j=l_1}^{lm} \nabla N_j \phi_j - \sum_{j=l_1'}^{l_n'} \nabla N_j T_j
\tag{96}
$$

The element current density can therefore be calculated by:

$$\overline{J}_1^e = -\sigma_1 \{ (\sum_{j=l_1}^{l_m} \nabla N_j \phi_j - \sum_{j=l_1'}^{l_n'} \nabla N_j T_j) - (\overline{V}_s \times \overline{B}_g) \} \tag{97}$$

where, ∇N_i $(i = l, m, n, s)$ can be calculated using equations (89) through (92).

In region, Ω_2:

In this region, no $(\overline{V} \times \overline{B})$ component and no potential jump are encountered. Hence, the current density of the element becomes:

$$\overline{J}_2^e = -\overline{\overline{\sigma}}_2 \cdot (\sum_{j=l_1}^{l_m} \nabla N_j \phi_j) \tag{98}$$

7 Example

In this work, an example (see Fig.2.5) is chosen to verify that the practicality and utility of the 3D-FE model developed in the previous sections. In Fig.2.5, we choose a cylinder as the moving object in place of the space station. Some geometric parameters and physical parameters are as follows:
the length of the cylinder, $L = 20 \ m$
the radius of the cylinder, $R = 5 \ m$
the radius of the outer sphere boundary, $R_0 = 40 \ m$
the flux density along the negative z-axis, $B_g = 0.45G = 0.45 \times 10^{-4} Wb/m^2$
the speed of the cylinder along the negative y-axis, $V_s = 8km/sec.$
the conductivity inside the cylinder, $\sigma_1 = 5.7 \times 10^7 \ 1/(\Omega \cdot m)$
the conductivity outside the cylinder, $\sigma_2 = 5.7 \times 10^5 \ 1/(\Omega \cdot m)$
The outer boundary condition in this example is assumed to be the natural boundary condition.

The 3D-FE gird with a total number of elements, NE=3456, and a total number of nodes, NN=669, is shown in Fig.2.6. An FE grid with a total number of elements, NE=28128, and a total number of nodes, NN=4963, is chosen for the FE computation, whose surface elements on the cylinder and outer boundary are shown in Fig.2.7. The equipotential lines and the current density distribution along the plane of the cross section ($z = 0, y \geq 0$) were plotted from the results of this FE model see Fig.2.8 and Fig.2.9, respectively. The numerical results of the current density component $\overline{J}_x$ vs radius on Plane x=0 are plotted in Fig.2.10. The numerical results of the scalar potentials located on the x-axis are plotted in Fig.2.11.

8 Conclusions and Possible Future Work

As a result of this investigation two technical papers on ballooning FE models and on twisted-pair transmission lines were presented at the IEEE INTERMAG-92 Conference, and were simultaneously published in the September issue on the IEEE Transactions on Magnetics (IEEE Trans. on Magn. Vol.30, No.5, 1992). These papers are included here in Appendix (III) and Appendix (IV), respectively.

Meanwhile, in order to obtain higher accuracy results regarding the present $(\overline{V}_s \times \overline{B}_g)$ problem formulated in this report, the asymptotic boundary conditions (ABCs) should be adopted instead of the natural boundary conditions. High order ABCs can improve the accuracy of the numerical results.

When the moving body is long and slender, a sphere shape outer boundary would be "storage memory intensive" and numerically inefficient. It would be highly desirable to choose an outer boundary that is conformal to the shape of the object. A formulation based on the ABCs should be derived for this 3D-FE scalar potential problem with an outer boundary of an arbitrary shape (an ellipsoid is one possibility).

In future work, the flux density distribution caused by the resulting pattern of induced current in the plasma and structure can be computed. This can be accomplished by a 3D-FE vector potential formulation using second order elements with the ABCs on the outer boundary, which should be designed to accommodate various shapes of the orbiting body under consideration.

References

[1] R. Mittra "Review of Absorbing Boundary Condition for Two and Three-Dimensional Electromagnetic Scattering Problems" *IEEE Trans. on Magn.*, Vol.25, No.4, July, 1989, pp 3034-3039

[2]Zienkiewicz and Talor *The Finite Element Method*, McGraw-Hill Book Company (UK) 1989

[3] S. Ratnajeevan H. Hoole *Computer-Aided Analysis and Design of Electromagnetic Devices*, Elsevier Science Publishing Co., Inc. 1989
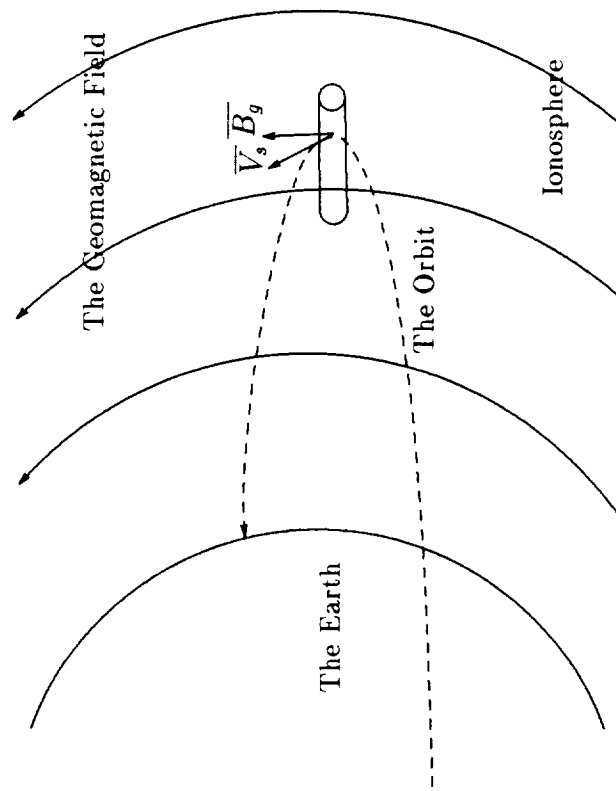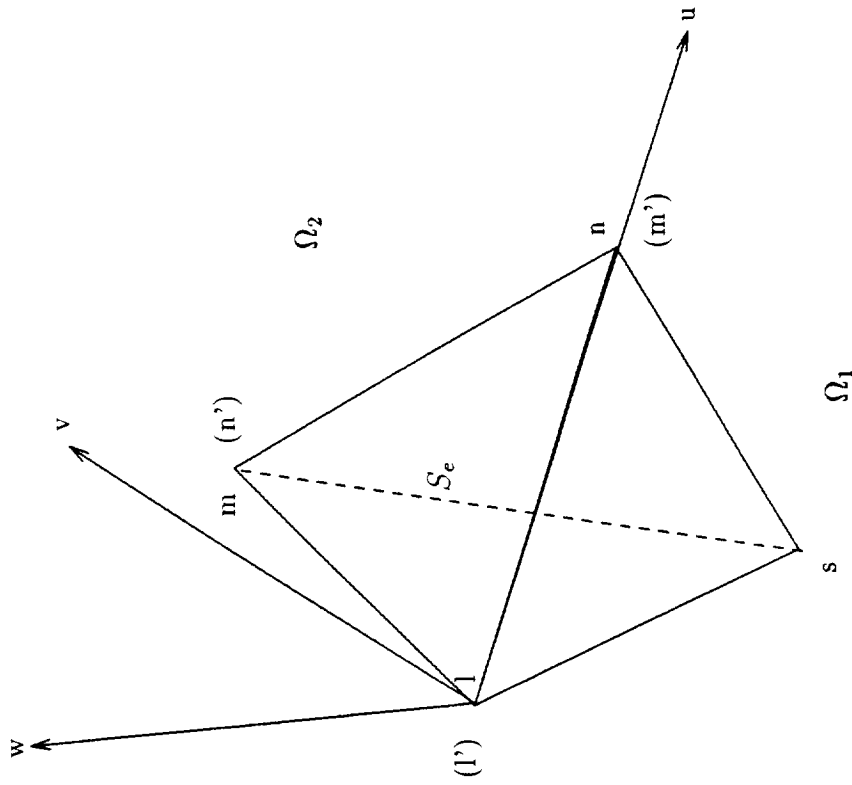
Figure 2.1   Orbital motion of Space Station Freedom in the Earth's geomagnetic field in the ionosphere.
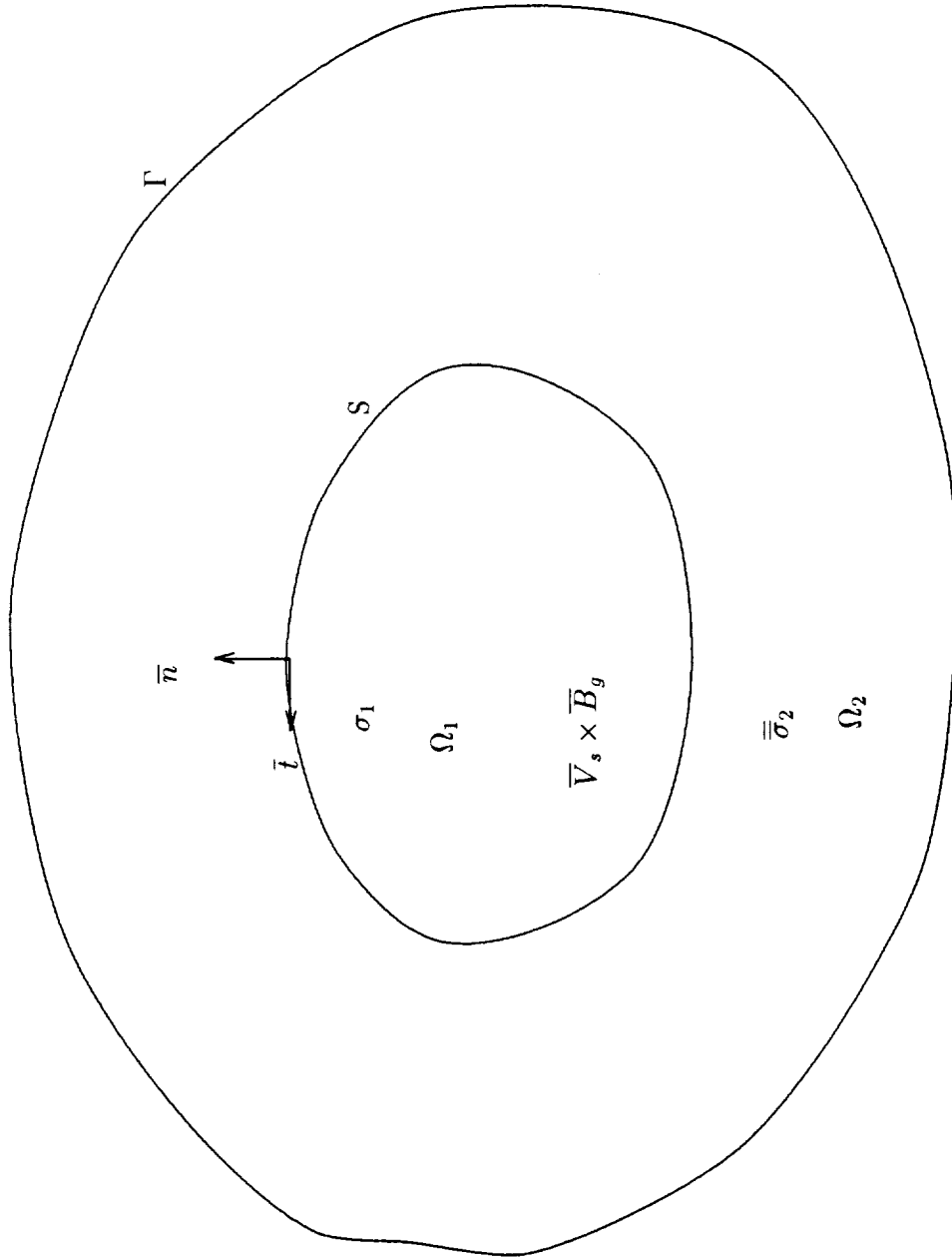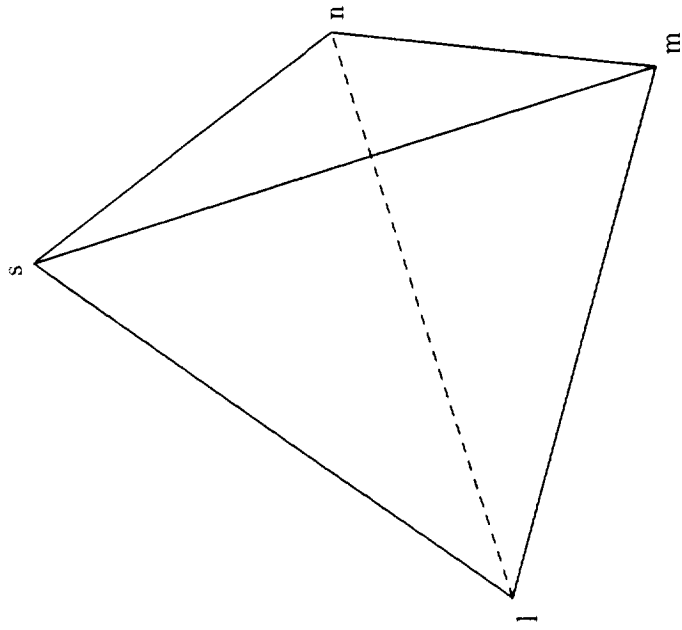
Figure 2.2   The partition of the problem region.

Figure 2.3 The first order tetrahedral surface element and local coordinate.
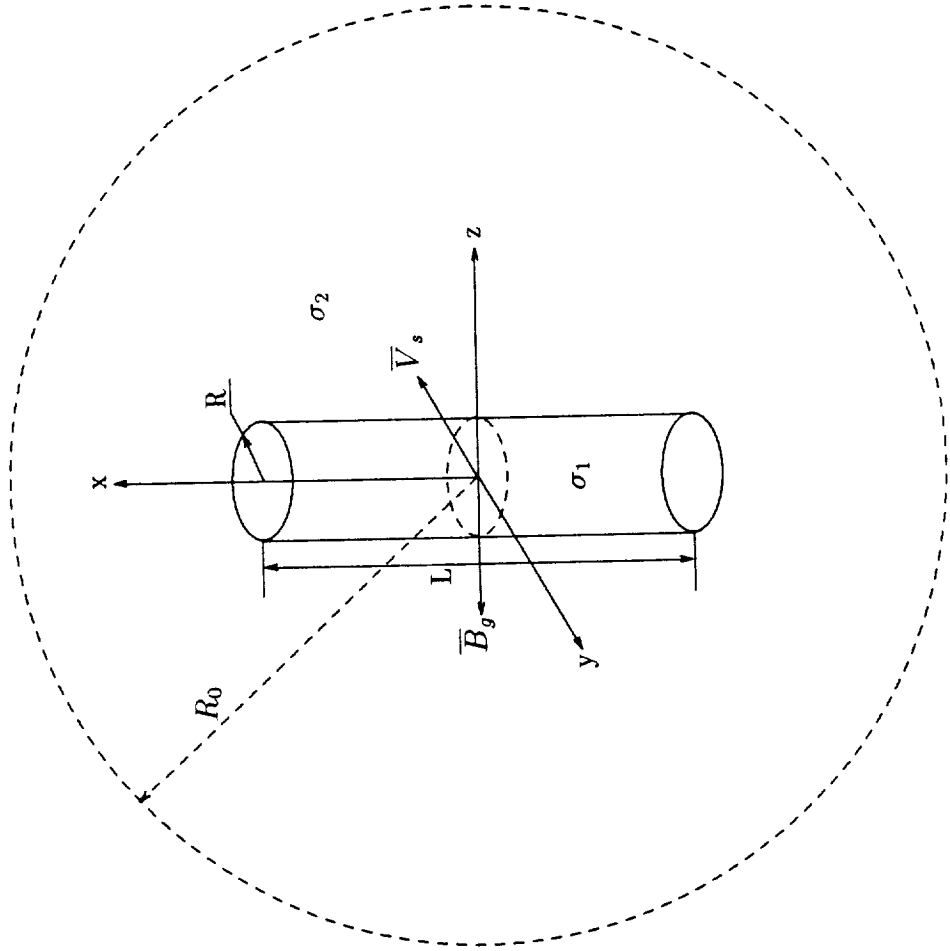
Figure 2.4   The first order tetrahedral element.

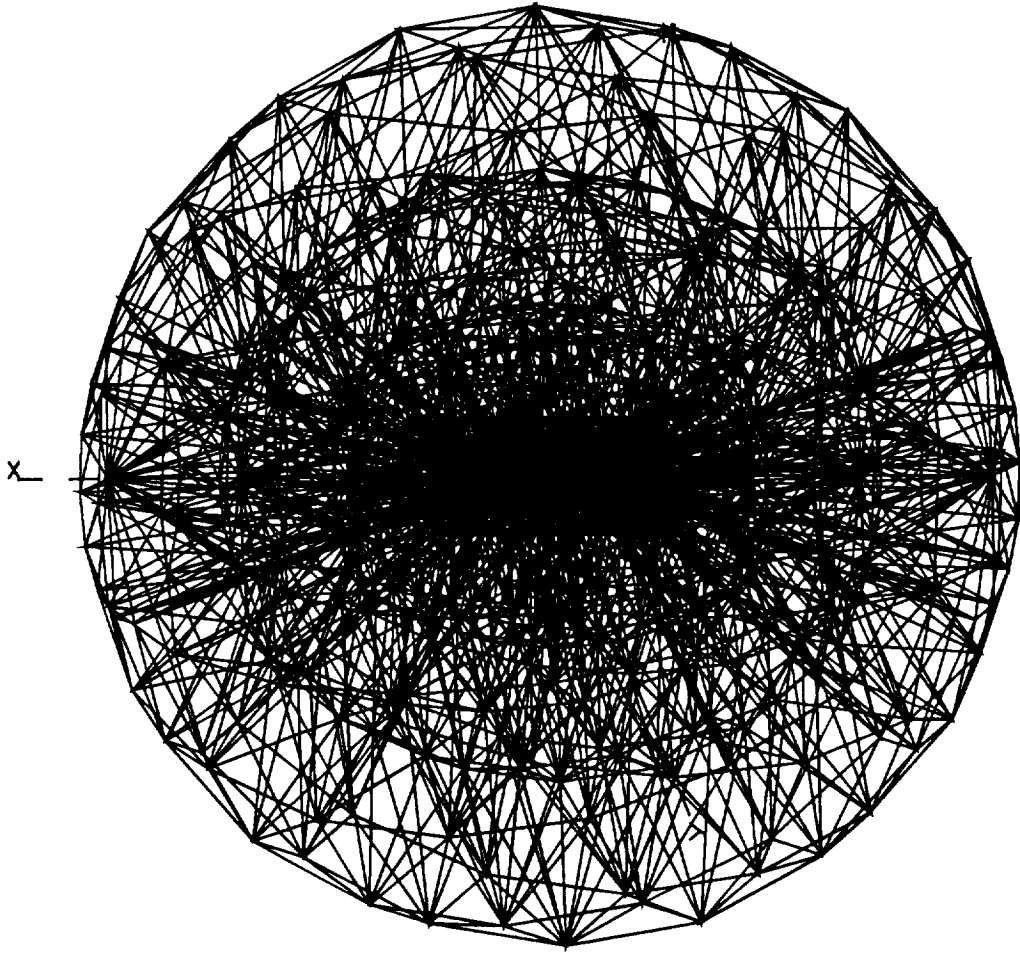**Figure 2.5**   Geometry of the example.

Figure 2.6   Tetrahedral element grid for a cylindrical object with a sphere outer boundary, for NE = 3456, NN = 669.
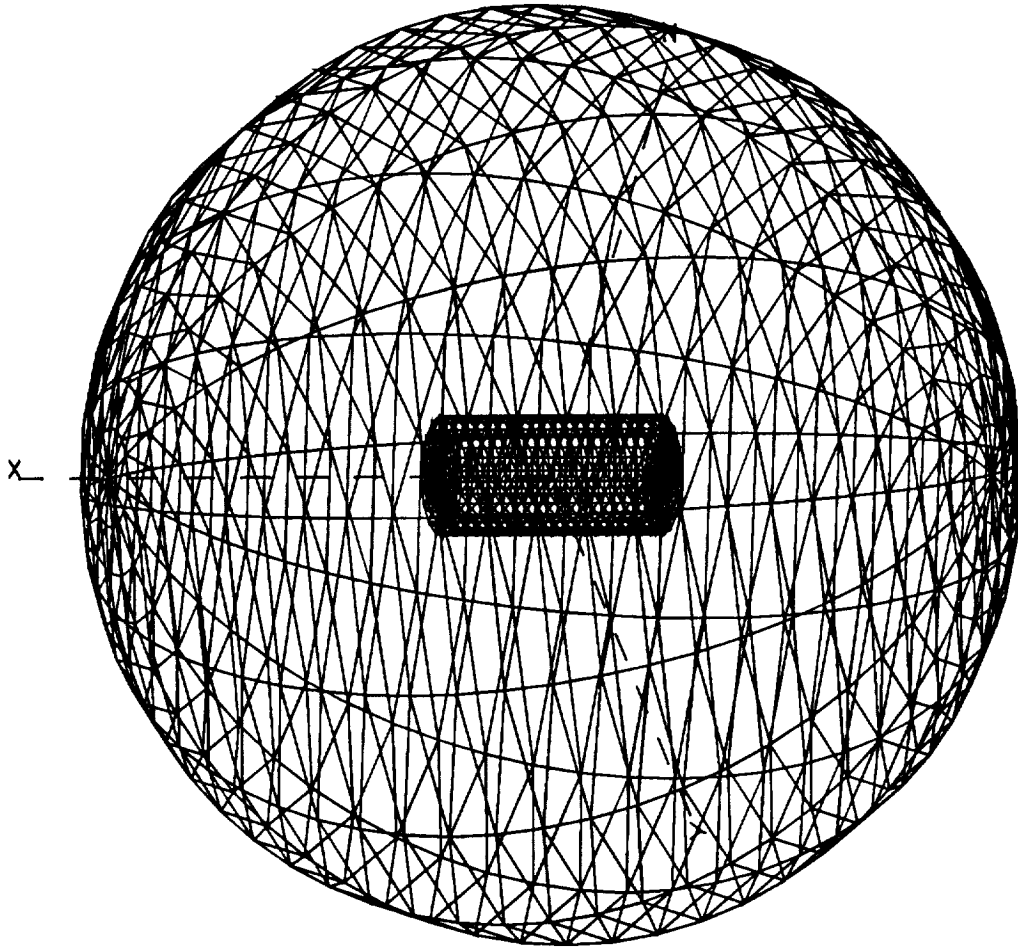
Figure 2.7   FE surface grid for a cylinder object with a sphere outer boundary.
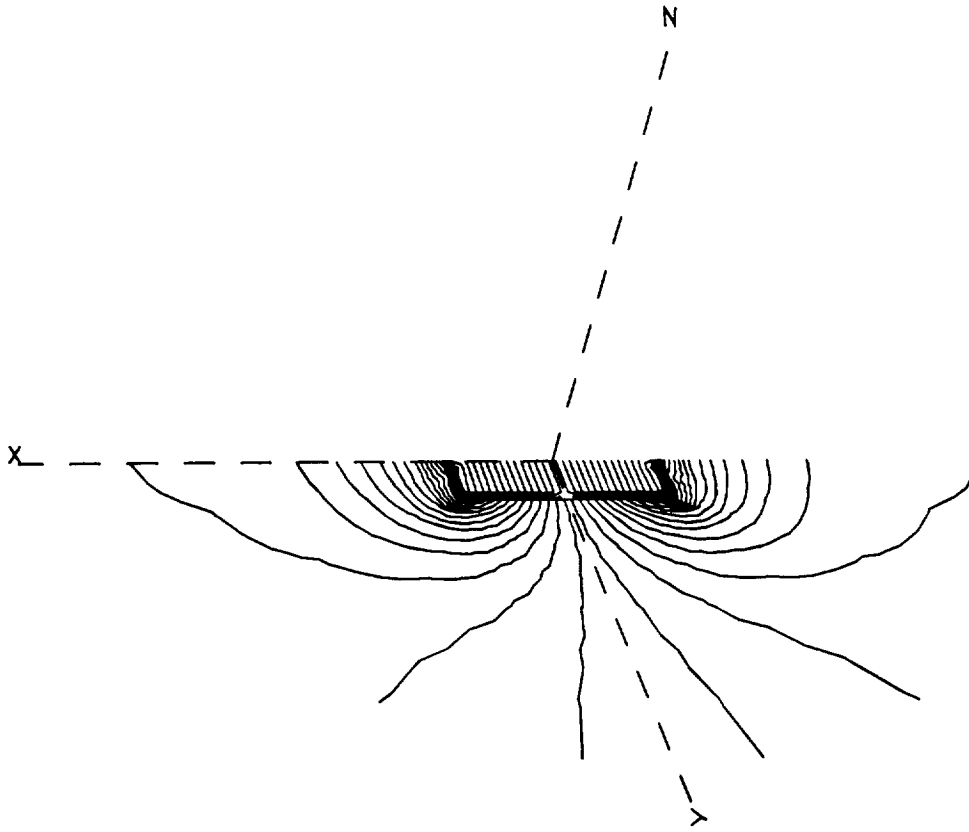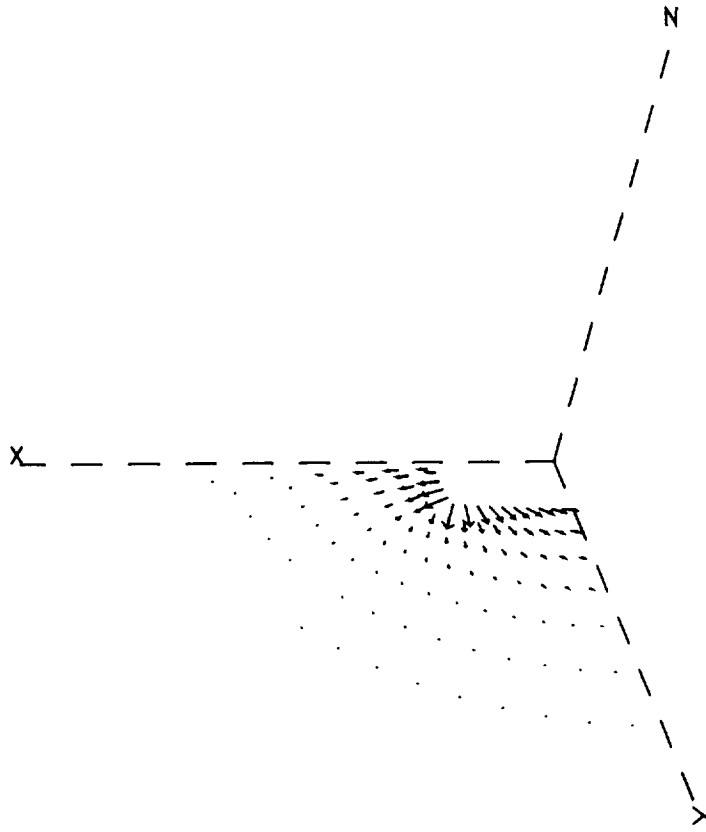
Figure 2.8   The equipotential lines on the cross section ($z = 0$, $y \geq 0$).

Figure 2.9 The current density distribution outside the object on the cross section $(z = 0, x \geq 0, y \geq 0)$.

The Current Density Component Jx on Plane X=0

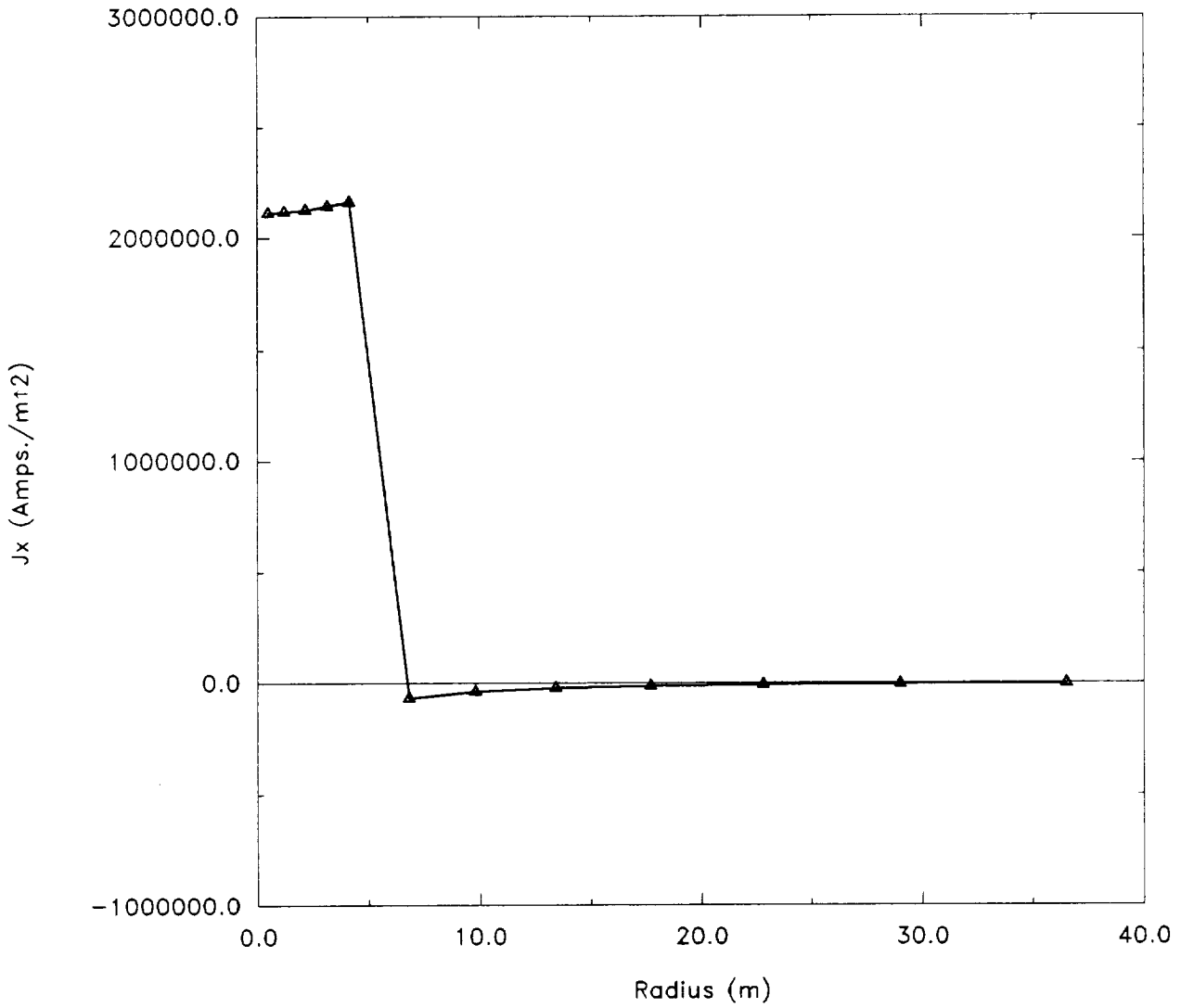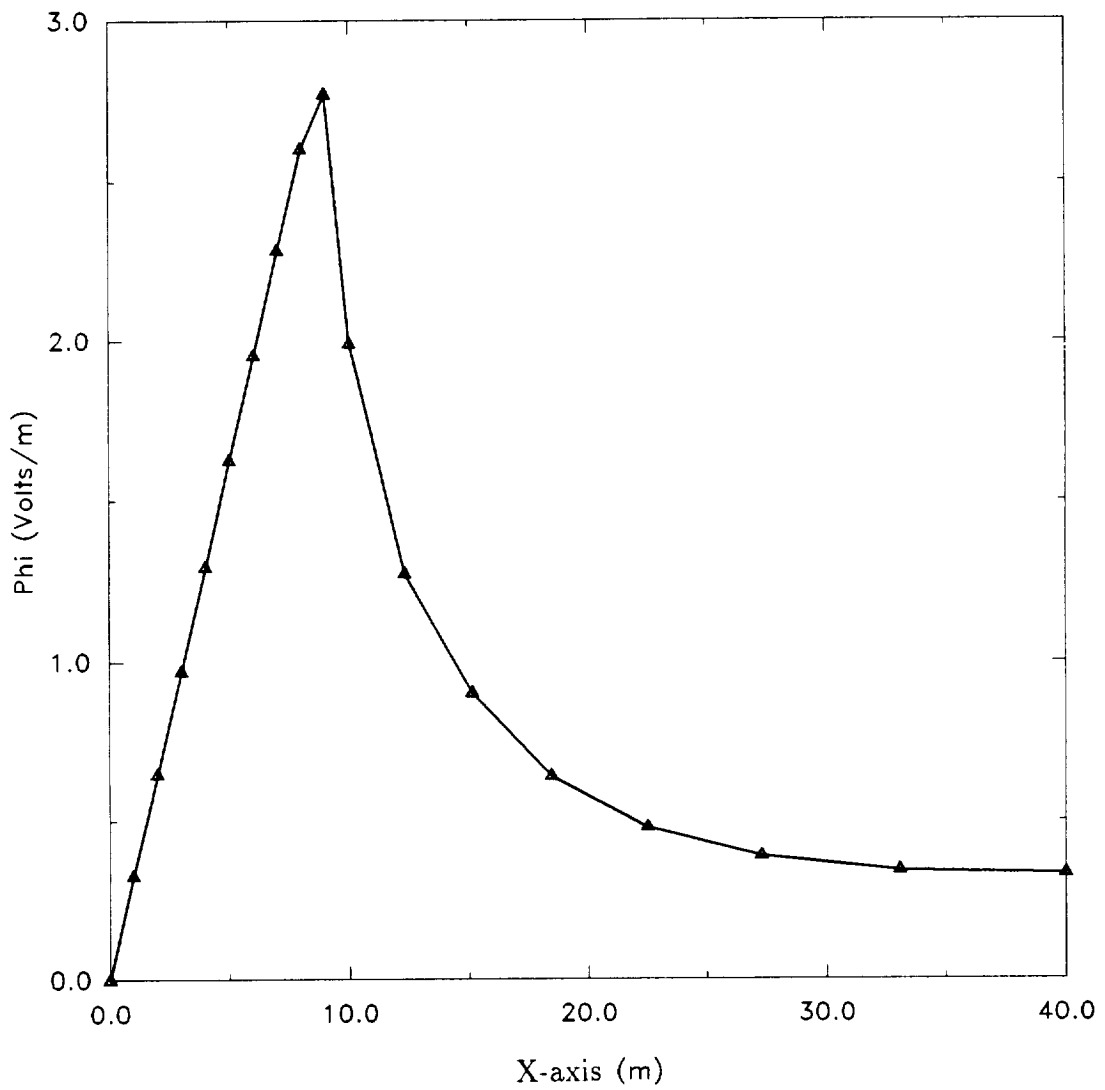Figure 2.10   The current density component J_x distribution on plane $x = 0$ with σ_1 = 5.7 × 10^7 1/Ω-m, σ_2 = 5.7 × 10^5 1/Ω-m.

The Scalar Potential on X—Axis

Figure 2.11   The scalar potentials on the x-axis with $\sigma_1 = 5.7 \times 10^7$ $1/\Omega$-m, $\sigma_2 = 5.7 \times 10^5$ $1/\Omega$-m.

30

3   Radiation Sources

This portion of the investigation centers on the development of computer models to calculate the radiation from simulated electromagnetic interference (EMI) sources on the space station.

Section 3.1 briefly describes the plasma environment of the ionosphere within the altitude range corresponding to the orbit of the space station. It is shown that the anticipated frequencies of potential EMI sources fall well below the plasma frequency. Therefore, radiation at these frequencies will be attenuated by the plasma. Method-of-moments analyses of the radiation by sources on a straight wire and on a simple model of the space station demonstrate that both the currents in the structure and the electric fields around the structure may be calculated. Calculated results are also shown for the simple model of the space station embedded in a zero-order-plasma. This plasma approximation includes the charged particle density at the altitudes of interest, but neglects the geomagnetic field, thereby resulting in an isotropic rather than an anisotropic plasma. The results show that while the plasma attenuates the radiation, induced currents in the structure nevertheless produce radiated fields that exceed those that would be present in the absence of the conducting space station structure. Software that can be used to visualize contour diagrams of the calculated electric field distribution around the simple model of the space station is described.

Section 3.2 describes the development of a wire-grid model of the space station that has been analyzed using the method-of-moments by the Electromagnetic Environmental Effects Laboratory at the Georgia Tech Research Institute. This is almost the same approach that the European Space Agency is using to predict EMI problems on their spacecraft. Calculations have been made for eight different cases comprising two source locations, two polarizations, and two frequencies, 20 KHz and 5 MHz. The calculated results show top view and side view contour graphs of the electric field for each case - a total of sixteen graphs. Software that can be used to visualize both the wire-grid space station model and contour diagrams of the calculated electric field distribution around the space station is described.

Section 3.3 briefly summarizes the available literature on plasma sheath waves. Excerpts from three recent publications, a journal article and two conference proceedings, are given. It has been shown (by others) that a region of low charge density, called a sheath, forms around a conducting object, like the space station, when it is embedded in the ionospheric plasma. A source on the conducting object can very efficiently transfer electromagnetic fields to distant locations by launching waves in the sheath region. The condition for transmission is the opposite of that for propagation in the ambient plasma as described in Section 3.1. Namely, sheath transmission is unattenuated for frequencies below the plasma frequency and is attenuated for frequencies above the plasma frequency. Sheath waves may therefore be an important factor in EMI analysis.

Section 3.4 briefly summarizes the available literature on finite-difference time-domain analyses of electromagnetic wave propagation in anisotropic plasmas. The

31

abstracts of three publications, two journal articles and a conference proceeding, are given. These new analysis tools may be important for predicting the propagation of EMI signals in realistic models of the ionospheric plasma, i.e., a plasma model that includes both the charged particles and the geomagnetic field.

3.1 Simple Wire Model of Space Station Freedom in a Zero-order Plasma

The space station will be embedded in the ionospheric plasma, a region of dense electric charge. As far as electromagnetic wave propagation in the ionosphere is concerned, the ionosphere can be modelled as an isotropic plasma if the geomagnetic field is neglected. Electromagnetic waves are then attenuated when their frequency is below the plasma frequency, but they propagate freely and unattenuated when their frequency is above the plasma frequency. Most importantly, the direction in which the wave is traveling is immaterial - exactly the same behavior occurs. However, when the geomagnetic field is considered, the plasma becomes anisotropic and the affect of the ionosphere on electromagnetic wave behavior depends on the direction of the electromagnetic wave relative to the direction of the magnetic field. All electromagnetic interference analyses to date have assumed an isotropic plasma, i.e., the geomagnetic field has been neglected. This assumption seems appropriate when what is needed is the basic behavior of electromagnetic interference in the presence of the plasma - to assume otherwise would greatly complicate any numerical calculations with little improvement in understanding the basic behavior of the interaction.

The key parameter in studying electromagnetic wave propagation in a plasma is the plasma frequency

$$\omega_p = \sqrt{\frac{Ne^2}{m_e \varepsilon_0}} \; , \tag{1}$$

where N is the electron density in electrons per m^3, e is the electron charge in Coulombs, m_e is the electron mass in kg, and ε_0 is the permittivity of free space. Although the ionosphere consists of both electrons and ions, most of the interaction occurs with the electrons because they have a much smaller mass, and therefore are more responsive to the influence of electric and magnetic fields. That is the reason that the plasma frequency is written only in terms of the electron charge and mass.

The variable factor in eq. (1) is the electron density N. Figure 3.1 shows the ionospheric charge density as a function of altitude for an equatorial orbit corresponding to the orbit of the space station. If only the electrons are considered, and an orbit altitude of 450 to 550 kilometers is assumed, it can be seen that $\log_{10} N$ falls in the range of 4.7 to 6.3 as shown in the outlined rectangular region in Fig. 3.1. This corresponds to an electron density N of 0.05×10^{12} to 2.0×10^{12} electrons per m^3.

Figure 3.2 shows the calculated plasma frequency, $f_p = 2\pi\omega_p$, for the assumed range of N. From the graph, it can be seen that the minimum plasma frequency of

2 Mhz corresponds to the minimum electron density. Since propagation occurs for frequencies above the plasma frequency and attenuation occurs for frequencies below the plasma frequency, attenuation is expected for all frequencies below 2 Mhz. A plane wave is attenuated by a factor of exp(-αr), where α is the attenuation factor in m^{-1} and r is the distance in m. The attenuation factor α is dependent upon the frequency of propagation ω relative to the plasma frequency ω_p according to

$$\alpha = \frac{2\pi}{\lambda} \sqrt{\left(\frac{\omega_p}{\omega}\right)^2 - 1} \quad . \tag{2}$$

Figure 3.3 shows the calculated attenuation in dB/m as a function of frequency for different electron densities. The attenuation factor increases with increasing electron density. For a given electron density, the attenuation is fairly constant until the plasma frequency is approached, at which point the attenuation drops to zero according to eq. (2).

The effect of the plasma on electromagnetic wave propagation is explicitly shown in Fig. 3.4. This shows the θ - component of the electric field radiated by a short dipole as a function of distance away from the dipole for free space (zero electron density) and for electron densities from 0.01×10^{12} to 1.0×10^{12} per m^3. It is clear that increased electron density results in increased attenuation. Here we have assumed that the near-field attenuation of the dipole fields occurs in a similar way as far-field attenuation.

The above has considered the effects of the plasma on electromagnetic wave propagation, but without the presence of the space station structure. The influence of physical structure can be incorporated by using the method of moments, a well-known numerical electromagnetic analysis method. The method of moments can be used to find the currents and the local electromagnetic fields about a conducting structure which has been excited by a current or voltage source. The calculation finds both the currents and the fields. In fact, the solution procedure first finds the currents and then calculates the fields radiated by these currents. As an example, Figure 3.5 shows a 100 m wire (divided into 34 segments for analysis) excited by a short monopole antenna at the left end. The current distribution in the wire is then calculated for a 20 KHz, 100 KHz, 1 MHz, and 5 MHz source for the free-space (no plasma) case. The calculated current distribution is shown in Fig. 3.6. At the lower frequencies of 20 and 100 KHz, the normalized current distribution is the same. The smooth decrease of the current from the maximum at the source end to zero at the far end is characteristic of an antenna that is short relative to a wavelength. The wavelength at 100 KHz is 3000 m, so the structure is about 0.033 wavelengths in length at this frequency. The length of the wire in terms of wavelengths is even shorter at 20 KHz. As the frequency increases to 1 MHz, the distribution changes only slightly, as the structure is now about 0.3 wavelengths in length. However, at 5 MHz, the structure is 1.67 wavelengths in length. Since we expect standing waves

to form with nulls every half wavelength, excitation at 5 Mhz should result in 1.67/0.5 or 3.3 standing wave cycles along the wire length. Figure 3.6 therefore shows the expected result. There are also fields radiated by the wire, but they are not shown here. However, it is important to recognize that the currents in the wire and the fields around the wire are coupled and both will be excited by a source on this or any other conducting structure.

Figure 3.7 shows a simple wire model of the space station for which near-field calculations have been made using the method of moments. The 100 m longtitudinal wire consists of 20 segments, with a one-volt source on the left-most segment. The source location was selected to simulate the switching associated with the photovoltaic solar panels. The two vertical wires, representing the habitation and laboratory modules, are each divided into 10 segments. The calculations account for the influence of the ionosphere by assuming a zero-order plasma environment. However, the effects of the plasma are incorporated only in the calculation of the radiated field and not in the calculation of the currents which produce the fields. Simple wire models like this are acceptable when the physical details of the actual structure are of a dimensional scale much less than a wavelength. At 1 MHz, the largest dimension of this model of the space station is only 0.33 wavelengths in length, so modelling with wires is justified.

Calculations were first made for the model in free space. Figure 3.8 shows the results for a 1 MHz source located at the left end of the structure, corresponding to the origin (x = 0, y = 0) in Fig. 3.8. The contour lines are in units of dB μV/m. The results show the field strength to be relatively strong around the source as expected. The strong fields at the opposite end of the structure from the source indicate that conducted currents in the structure are an extremely efficient mechanism for transferring the influence of the source to other points on the structure. Based on the rapid decrease of the fields in the free-space region around the source, normal free-space considerations would predict fields at the far end of the stucture to be an order of magnitude less than what is calculated with the structure present. This is the reason why the conducting structure plays such an important role in electromagnetic interference analysis - it provides a current pathway for electromagnetic fields.

The calculations were repeated using a zero-order plasma environment with an electron density N of 0.1×10^{12}, corresponding to a plasma frequency of about 3 MHz. These results are shown in Fig. 3.9 and the attenuating effect of the plasma is obvious as the fields around the space station structure are greatly reduced (recall that the units are dB μV/m). However, the fields very close to the structure are still significant. This is once again a result of the fields being transferred to other locations on the structure via the conducted currents. The method of moments solution for the plasma case did not use the plasma in the calculation of the currents (the structure current is the same in the calculation of Figs. 3.8 and 3.9), but only in the calculation of the fields radiated by the current. Were the plasma included in the current calculation, attenuation of the current would be expected and even lower fields close to the structure should result. Nevertheless, it is clear that the

conducting structure plays a significant role in producing fields close to the structure that are substantially greater than would be expected from consideration of radiation effects alone.

Computer Visualization

The calculated method-of-moments results in Figs. 3.8 and 3.9 may be viewed on a color monitor. An IBM-compatible PC with 512 Kb memory and (preferably) a hard disk is required. A graphics program called TOPO, licensed from Golden Software, Inc., may be used.

First create a directory on the hard disk called TOPO and change to this directory. Then insert Disk #1 into the 3.5" floppy disk drive, switch to the floppy disk drive, change to directory TOPO, and copy all files to the hard disk (usually drive C:). Then switch back to the hard disk. The contour graphs may be generated as follows:

type topo/cmd=fs (upper or lower case)

when the program is loaded, press F2 to display Fig. 3.8 (free-space result)

press ESC when finished viewing

press ESC and RETURN to exit the graphics program

repeat the above except type topo/cmd=zop to display Fig. 3.9 (zero-order plasma result)

3.2 Method-of-Moments Wire-Grid Model of Space Station Freedom

The method-of-moments may be used to find the conducted currents and fields radiated from sources on the space station. Early work used a simple wire model embedded in a zero-order plasma to determine the near-field electric fields. The model was then improved by more accurate modelling of the habitation/laboratory module and the addition of solar panels. The latest model is shown in Fig. 3.10. This model is constructed using a wire mesh with 720 wire segments.

It is interesting to note that the European Space Agency is using the same electromagnetic analysis technique to develop EMC models of spacecraft (ESA report dated 8-28-91). Specifically, the method of moments is used to calculate the currents and the near electric field for a spacecraft excited by a voltage source. The method uses triangular surface patches rather than a wire grid to model the structure. The referenced report indicates that future work will include time-domain solutions, excitation by current sources as well as voltage sources, and the capability to include

35

dielectric materials as well as conducting surfaces. This work has apparently not included the effects of a surrounding plasma, probably because the applications currently being considered involve satellites in orbit above the ionosphere, in which case free space is a reasonable assumption.

The wire-grid model of the space station has been analyzed by the Electromagnetic Environmental Effects Laboratory at the Georgia Institute Research Institute using the General Electromagnetic Model for the Analysis of Complex Systems (GEMACS) computer program, which is a commercial method-of-moments electromagnetic analysis program. The program assumes free-space conditions, so the presence of the ionospheric plasma is not accounted for.

Four sets of calculations have been made, one for each of four different source configurations, two locations and two polarizations, as shown in Fig. 3.10 that are labelled #1, #2, #3, and #4. Two source frequencies, 20 KHz and 5 MHz, are considered for each source location and the distribution of the electric field is displayed in two planes, the x = 0 plane (Side view) and the z = 0 plane (Top view), as defined in Fig. 3.10. A total of 16 calculations have been made and graphs of the results are enclosed in this report as Figs. 3.11 - 3.26. The key to the graphs is shown in Table I.

Each of the graphs shows contours of electric field strength in dB μV/m for a one Volt source at the locations shown in Fig. 3.10. The reference for the dB scale differs from that used in Figs. 3.8 and 3.9 in that the reference level (0 dB) is set at the source resulting in a relative dB scale, whereas the simple wire model results displayed in Figs. 3.8 and 3.9 were on an absolute basis. The only practical difference is that the contours displayed here show negative dB values.

While calculations have been made for 20 KHz and 5 MHz (the 250th harmonic of 20 KHz), the 20 KHz results are of the most interest. The 20 KHz results for the source at location 1, top (file C20_T1) and side (file C20_S1) views, show the locations of high and low field strength. In particular, they show, as in the previous results for a simple wire model, that the presence of the conducting structure results in higher electric fields away from the source than would exist if the structure were not present. As previously explained, electric currents in the structure serve as a transfer mechanism for the electric fields.

<u>Computer Visualization</u>

The model shown in Fig. 3.10 may be viewed and rotated on a color monitor. An IBM-compatible PC with 512 Kb memory, (preferably) a hard disk, and a mouse is required. A freeware program called 3dv may be used.

First create a directory on the hard disk called 3D and switch to this directory. Then insert Disk #1 into the 3.5" floppy disk drive, switch to directory 3D, and copy all files to the hard disk (usually drive C:). The model may be viewed as follows:

type 3dv (upper or lower case)

36

use the mouse to click on the correct graphics mode (if necessary)

use the mouse to click on the ○ bullet to the left of FILE

use the mouse to click on SSF.3DV

use the mouse to click on the ○ bullet to the left of SHOW

rotate the model by moving the mouse

when through viewing, click either mouse button

use the mouse to click on the ○ bullet to the left of EXIT

The 16 calculated method-of-moments results for the wire-grid model may be viewed on a color monitor. An IBM-compatible PC with 512 Kb memory, (preferably) a hard disk, and a mouse is required. A graphics program called GraphTools, licensed from 3-D Visions Corporation, may be used.

First create a directory on the hard disk called GT and switch to this directory. Then create a subdirectory on the hard disk called TMP. Then insert disk #2 into the 3.5" floppy disk drive, switch to the floppy disk drive, change to directory GT, and copy file GTOOL.EXE to the hard disk (usually drive C:). Then switch back to the hard disk and change to subdirectory TMP. Then switch back to the floppy disk drive and change to subdirectory TMP. Copy all 33 files in TMP to the hard disk (usually drive C:). Then switch back to the hard disk and change to directory GT. Run program GTOOL to create the GraphTools graphics package. When the program has finished running, delete GTOOL.EXE. The contour graphs may be viewed as follows:

type gt (upper or lower case)

from the menu, use the mouse to click on File

use the mouse to click on Directory

use the mouse to click on OK

use the mouse to click on File

use the mouse to click on Load

press F3 to view the available files

use the mouse to click on the file that is to be plotted (see Table I)

use the mouse to click on OK

use the mouse to click on Redraw

to view another file, click on File, Load, and press F3 as before

use the mouse to click on Quit when finished

3.3 Sheath Waves - A Summary of the Recent Literature

J. J. Laurin, G. A. Morin, and K. G. Balmain, "Sheath wave propagation in a magnetoplasma," Radio Science **24**, pp. 289-300, 1989. (Complete paper in Appendix I.)

> "It has been understood by many authors that the presence of a low electron density sheath surrounding an antenna immersed in isotropic plasma provides a propagation region for electromagnetic waves, a situation that is of particular interest at low frequencies (signal frequency ω < plasma frequency ω_p) where the ambient plasma is cut off for uniform plane waves. In this case, the metal-sheath-plasma region becomes analogous to a waveguide in which surface waves, so-called sheath waves, may be excited and propagate over sufficiently long distances ... also provide a possible mechanism for locally generated electromagnetic waves to propagate between widely separated points on large spacecraft in the ionosphere."

G. B. Murphy and H. B. Garrett, "Interactions between the Space Station and the environment - a preliminary assessment of EMI," Proceedings of the 3rd Annual Workshop on Space Operations Automation and Robotics, Johnson Space Center, pp. 493-507, March 1990.

> "If the structure is conductive it will have a significant sheath surrounding it due to the **v** × **B** motional potential. This sheath has been shown to be capable of conducting noise over large distances very efficiently. Sheath waves are guided waves that are conducted along conductors surrounded by sheaths much like waves in a coaxial cable transmission line. Anywhere sheaths overlay, the waves can propagate. The significance of this is that noise generated locally can be conducted along Space Station structures to other cables which may be sensitive to this frequency. Unless the sheath is forced to collapse, the waves propagate with little attenuation. Therefore, as a worst case scenario,

38

we assume that cables placed anywhere externally on the Space Station may be within a sheath which is connected to a source of noise via the structure-sheath coax transmission line."

K. G. Balmain, H. G. James, and C. C. Bantin, "Magnetoplasma sheath waves on a conducting tether in the ionosphere, with applications to EMI propagation on large space structures," Proceedings of the 4th Annual Workshop on Space Operations Automation and Robotics, Johnson Space Center, pp. 646-654, January 1991. (Complete paper in Appendix II.)

"The evidence suggests that, on any large structure in low earth orbit, transient or continuous-wave electromagnetic interference, once generated, could propagate over the structure via sheath waves, producing unwanted signal levels much higher than in the absence of the ambient plasma medium."

3.4 Finite-Difference Time-Domain Modeling of the Ionosphere

T. Kashiwa, N. Yoshida, and I. Fukai, "Transient analysis of a magnetized plasma in three-dimensional space," IEEE Trans. Antennas Propag. 36, pp. 1096-1105, 1988.

Abstract

In recent years electromagnetic analyses of magnetized plasma have become important in various fields. Because of gyroelectric anisotropy with dispersion characteristics, the analysis is complicated, and three-dimensional treatment is indispensable. For efficient three-dimensional analyses in the time domain, the finite-difference time-domain method and the transmission-line-matrix method are generally used. However, until now these methods do not seem to have been applied to gyrotropic anisotropy with dispersion in the time domain. A new method was recently proposed for transient analysis in three-dimensional space based on the equivalent circuit of Maxwell's equations and formulation by the Bergeron method. In this method, magnetized cold plasma, that is, gyroelectric anisotropy with dispersion, is formulated by adapting the trapezoidal rule to the characteristic equation of motion of the plasma in the time domain. The formulation of the magnetized cold plasma in three-dimensional space and in the time domain by the present method is described. The two principal problems, transverse and longitudinal propagation, are studied. By examining these results, the validity of this formulation is demonstrated.

R. J. Luebbers, F. Hunsberger, and K. S. Kunz, "A frequency-dependent finite-difference time-domain formulation for transient propagation in plasma," IEEE Trans. Antennas Propag. **39**, pp. 29-34, 1991.

Abstract

Computation of transient electromagnetic propagation through plasma has been a difficult problem. Frequency domain solutions are available for one or two dimensions and stratified plasma geometries. Transient solutions have been obtained via transformations to the time domain, or by microscopic solution of the equations of motion of the charged particles. The finite-difference time-domain (FDTD) method is capable of explicitly computing macroscopic transient electromagnetic interactions with general three-dimensional geometries. However, previous FDTD formulations were not capable of analyzing plasmas for two reasons. First, FDTD requires that at each time step the permittivity and conductivity be specified as constants that do not depend on frequency, while even for the simplest plasmas these parameters vary with frequency. Second, the permittivity of a plasma can be negative, which can cause terms in FDTD expressions to become singular. A new FDTD formulation for frequency dependent materials $(FD)^2TD$ has been developed, which removes the above limitations. In a previous paper $(FD)^2TD$ was applied to computation of transient propagation through a polar dielectric. In this paper, we show that $(FD)^2TD$ may also be applied to compute transient propagation in plasma when the plasma can be characterized by a complex frequency-dependent permittivity. While the computational example presented in this paper is for a pulse normally incident on an isotropic plasma slab, the $(FD)^2TD$ formulation is fully three-dimensional. It can accomodate arbitrary transient excitation, with the one limitation that the excitation pulse must have no zero frequency energy component. Time-varying electron densities and/or collision frequencies could also be included. The formulation presented here is for an isotropic plasma, but extension to anistropic plasma should be fairly straightforward.

P. M. Franke and L. J. Nickisch, "Finite Difference - Time Domain solution of the Maxwell equations for the dispersive ionosphere," Proceedings of the 1991 APS/URSI International Symposium, London, Ontario, p. 85, June 1991.

Abstract

The Finite Difference - Time Domain (FDTD) technique is a conceptually simple, yet powerful method for obtaining numerical solutions to

electromagnetic propagation problems. The application of FDTD methods to problems in ionospheric radiowave propagation is, however, complicated by the dispersive nature of the ionospheric plasma. In the time domain, the electric displacement is the convolution of the dielectric tensor with the electric field, and this convolution is untractable in the nearest neighbor FDTD approach.

This difficulty can be avoided by returning to the constitutive relations from which the dielectric tensor is derived. By integrating these differential equations simultaneously with the Maxwell equations, dispersion (and absorption) is fully incorporated. The method is shown to be accurate by comparing to a known analytic solution for a special case.

IONOSPHERE CHARGE DENSITY

1986 International Reference Ionosphere
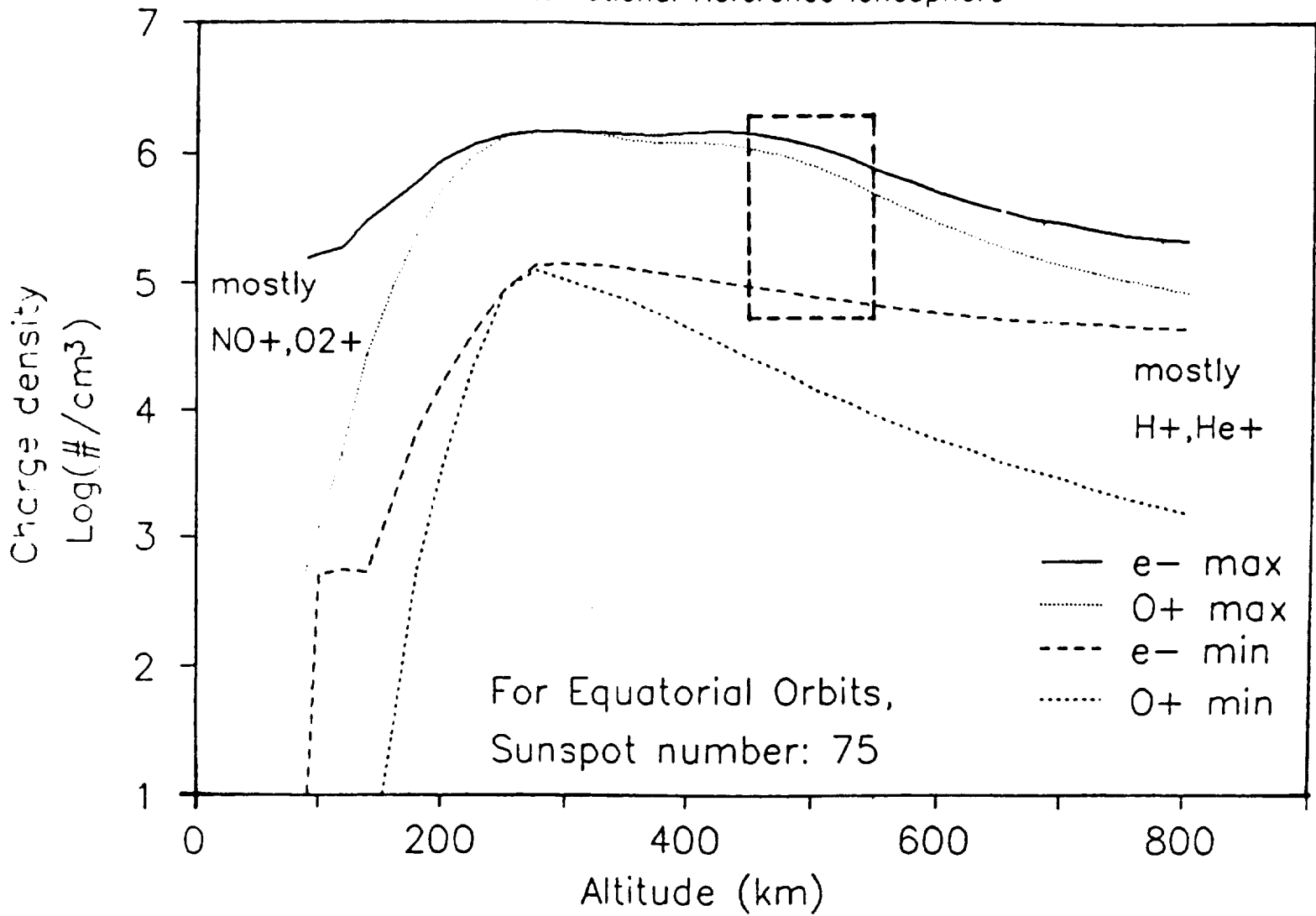
Fig. 3.1 Ionospheric charge density as a function of altitude.
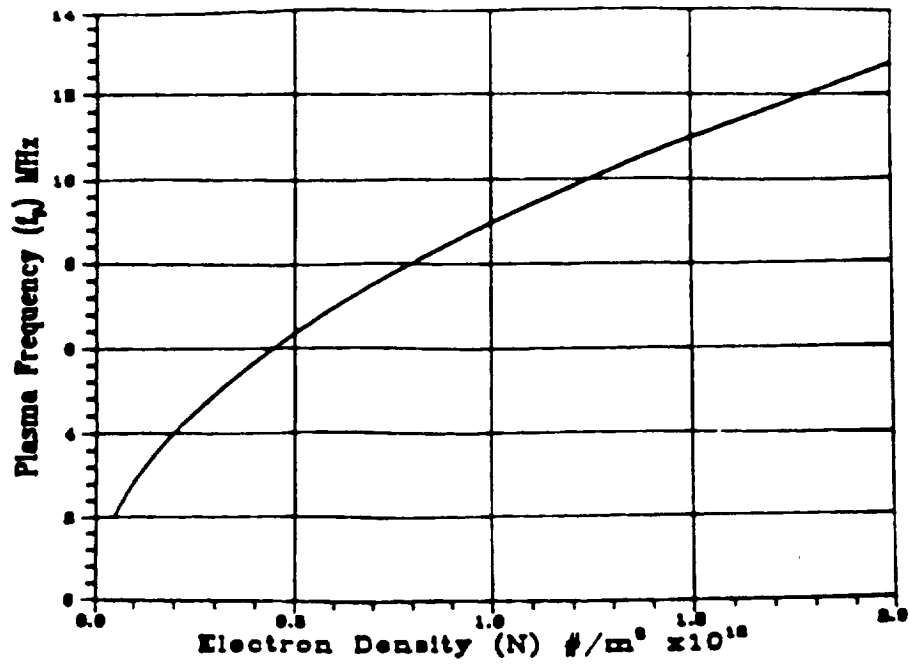
Fig. 3.2   Plasma frequency f_p versus electron density N.
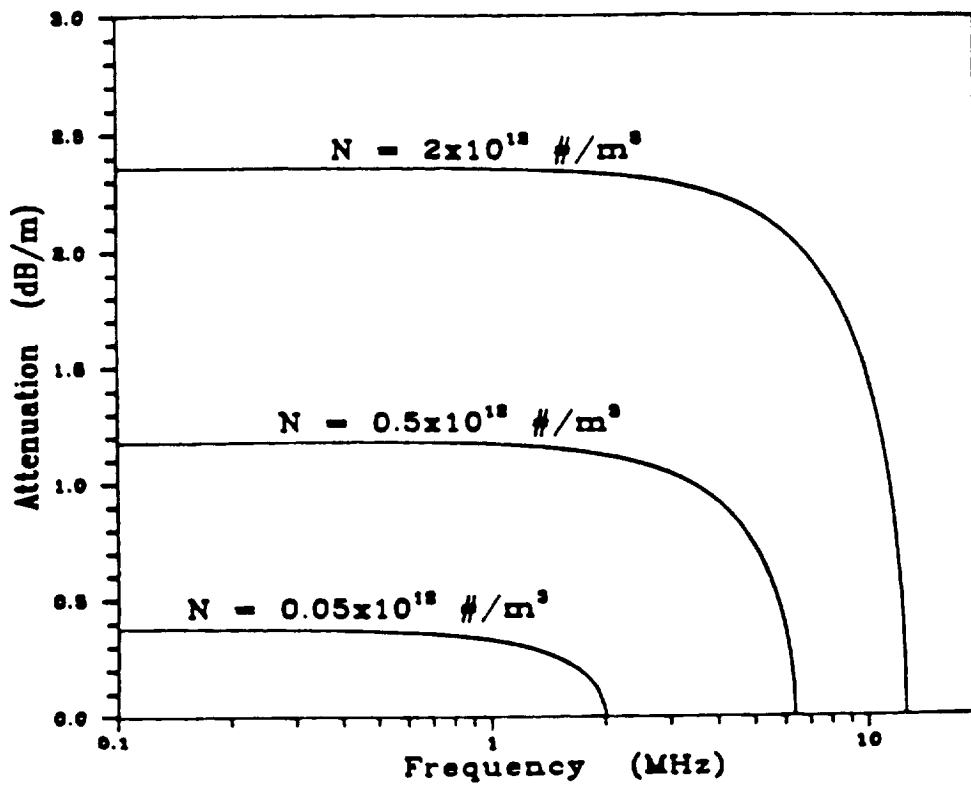
Fig. 3.3   Attenuation vs frequency for specified electron densities.
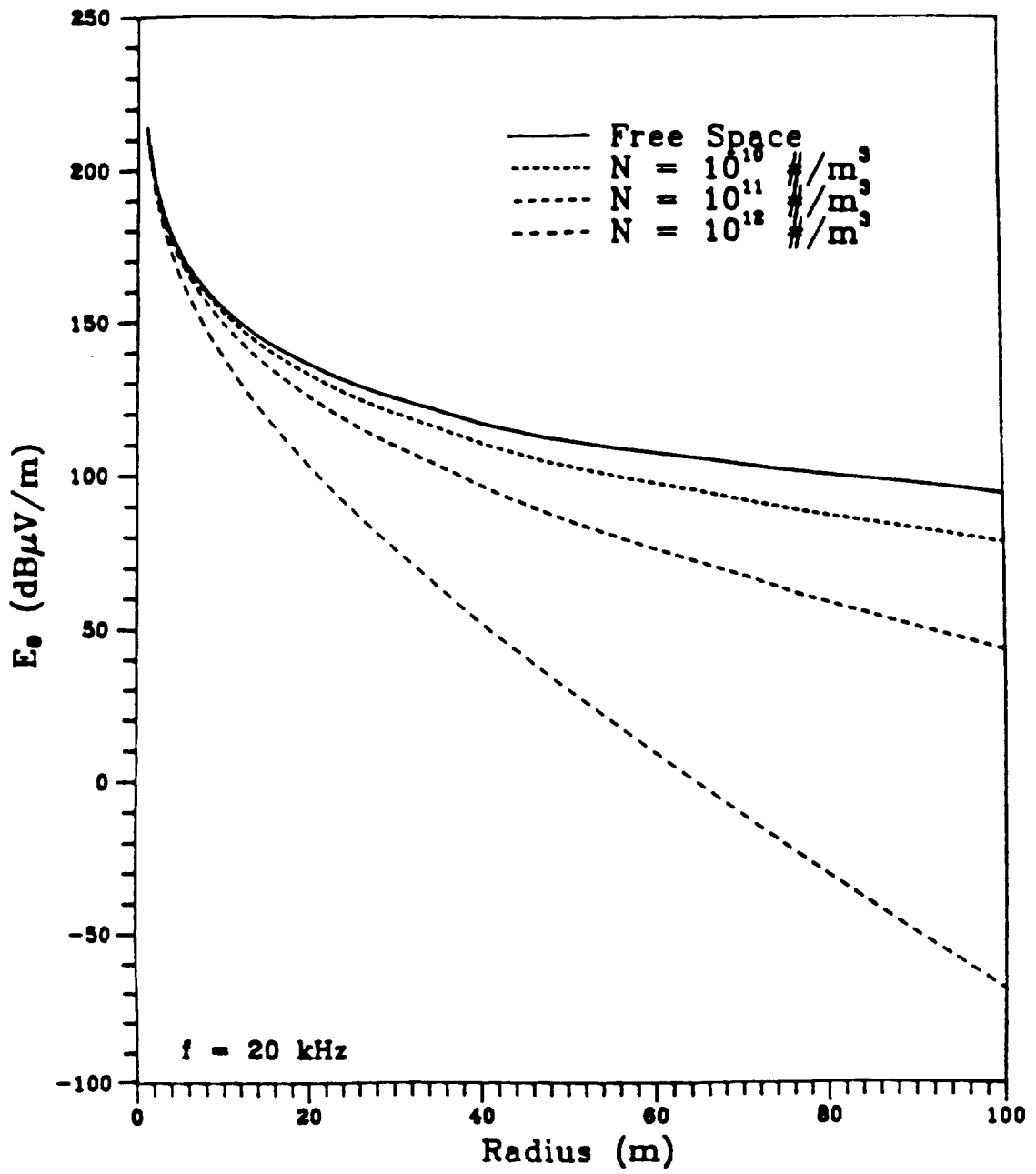
Fig. 3.4   Effect of varying the electron density on the electric field.
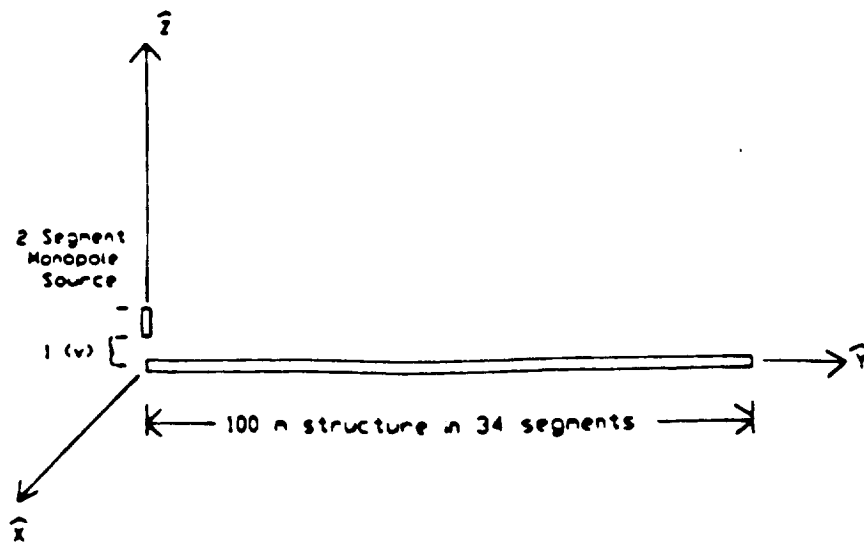
Fig. 3.5   Wire model with a short monopole antenna excited at one end.
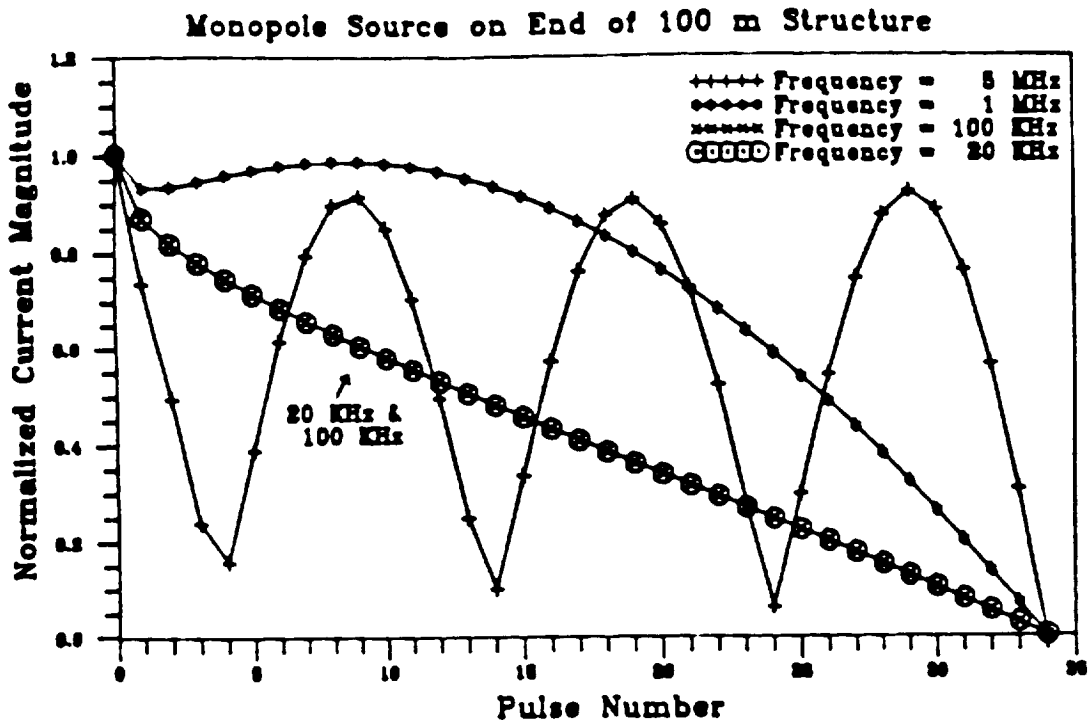
Fig. 3.6   Current along a 100 m wire with a monopole source at one end.
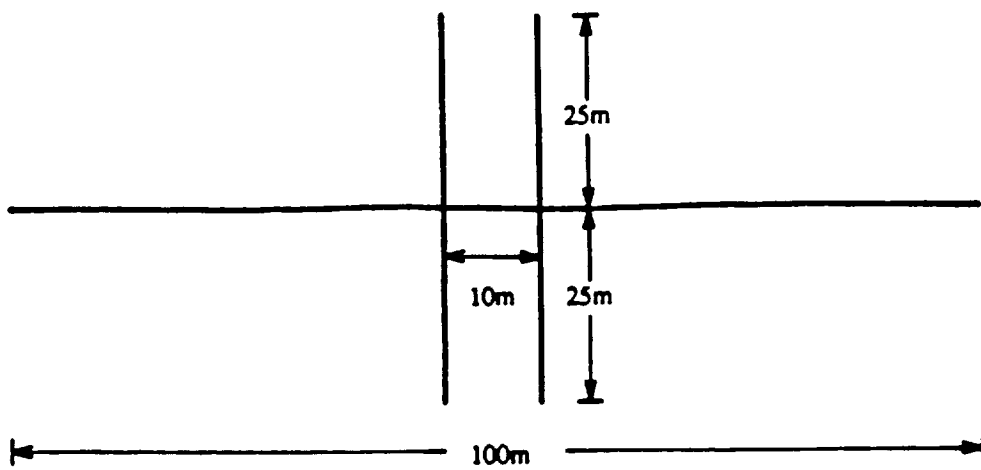
Fig. 3.7   Simple wire model of Space Station Freedom.
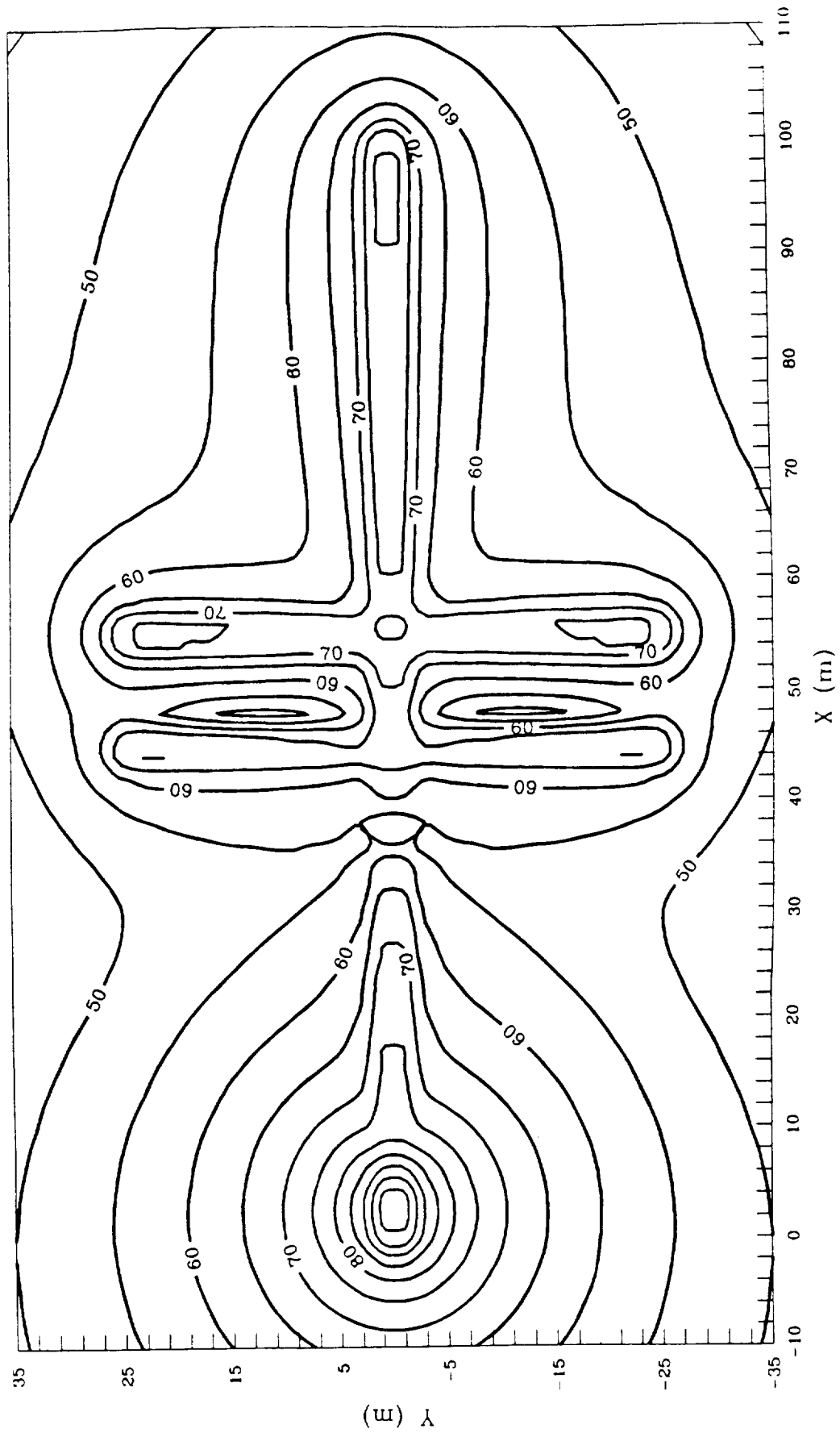
Fig. 3.8 Electric field intensity in dB μV/m from a 1 V, 1 MHz source on the simple model of the space station in a free-space environment.
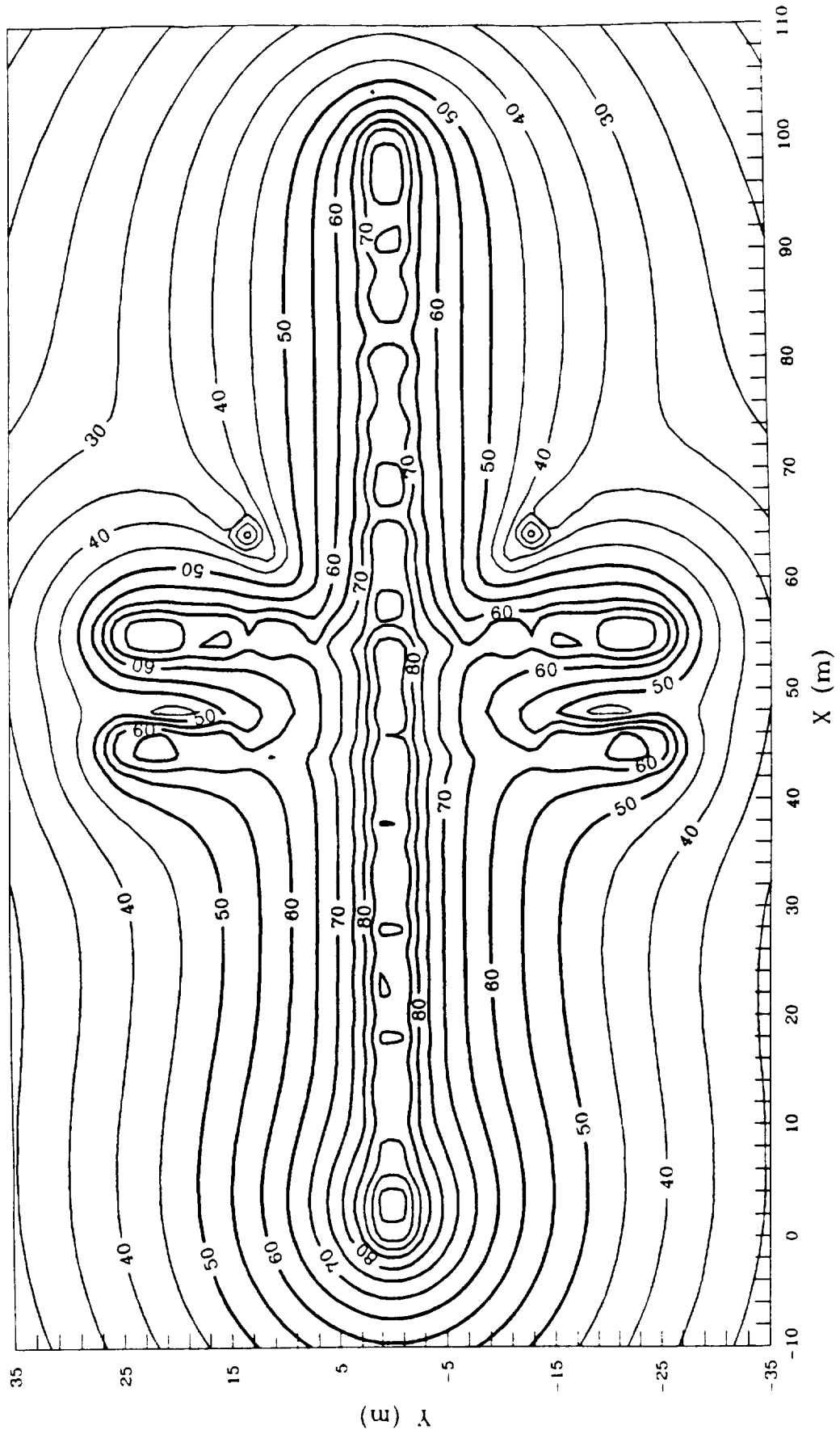
Fig. 3.9   Electric field intensity in dB µV/m from a 1 V, 1 MHz source on the simple model of the space station in a zero-order plasma environment.
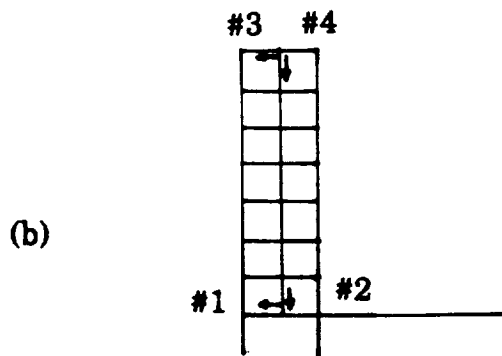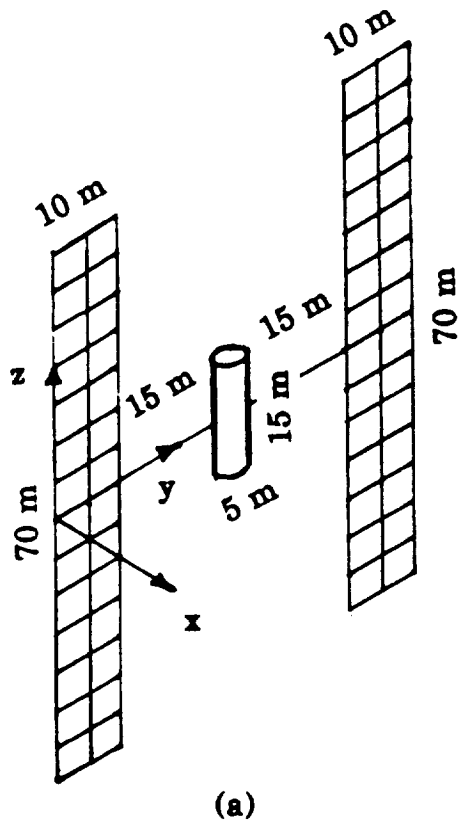
Fig. 3.10   (a) Wire-grid model of the space station. (b) Section of solar panel showing the location of the two sources and the two polarizations.

Electric Field Intensity in Normalized dB
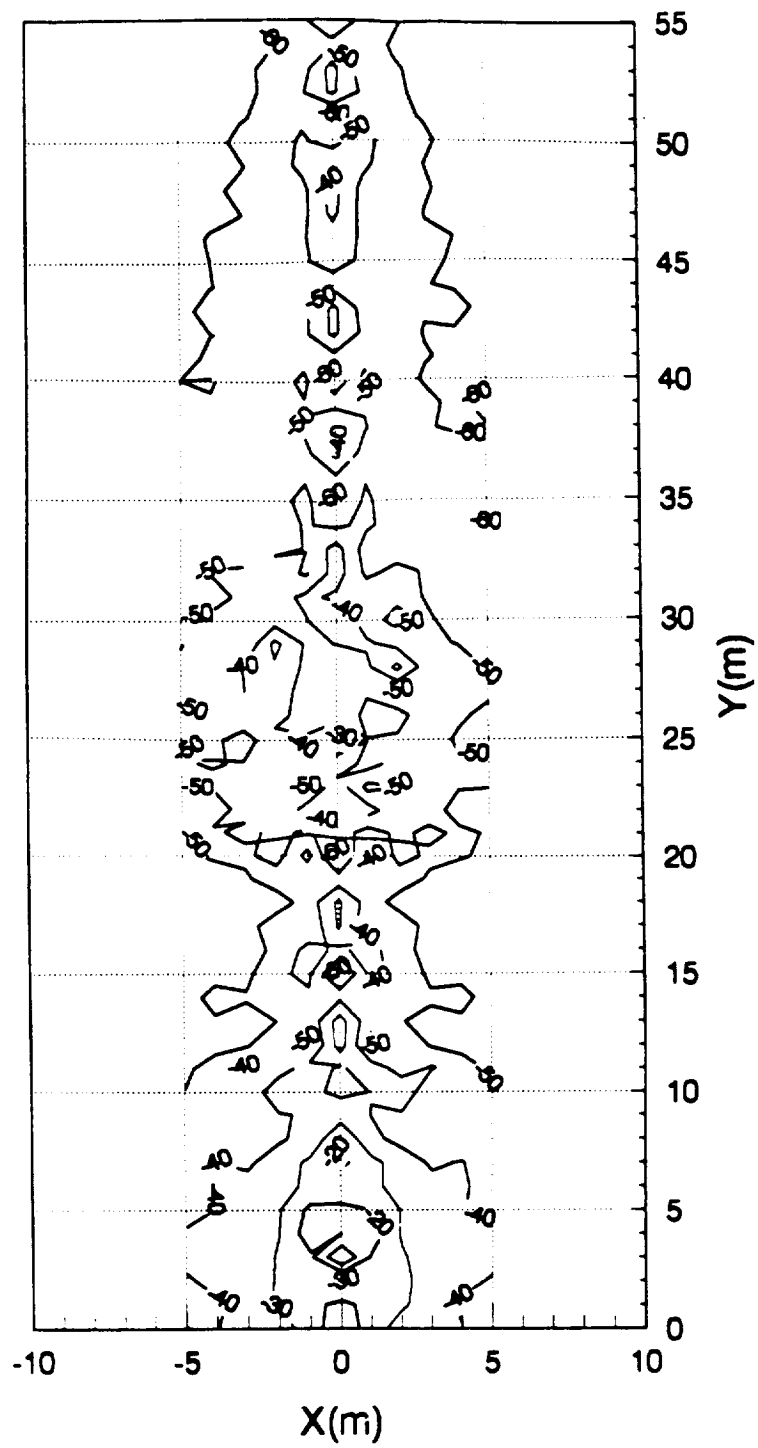at 5 MHz with Z = 0 (720 seg model/Source at Pos 1)
(Max = 0.325 V/m)
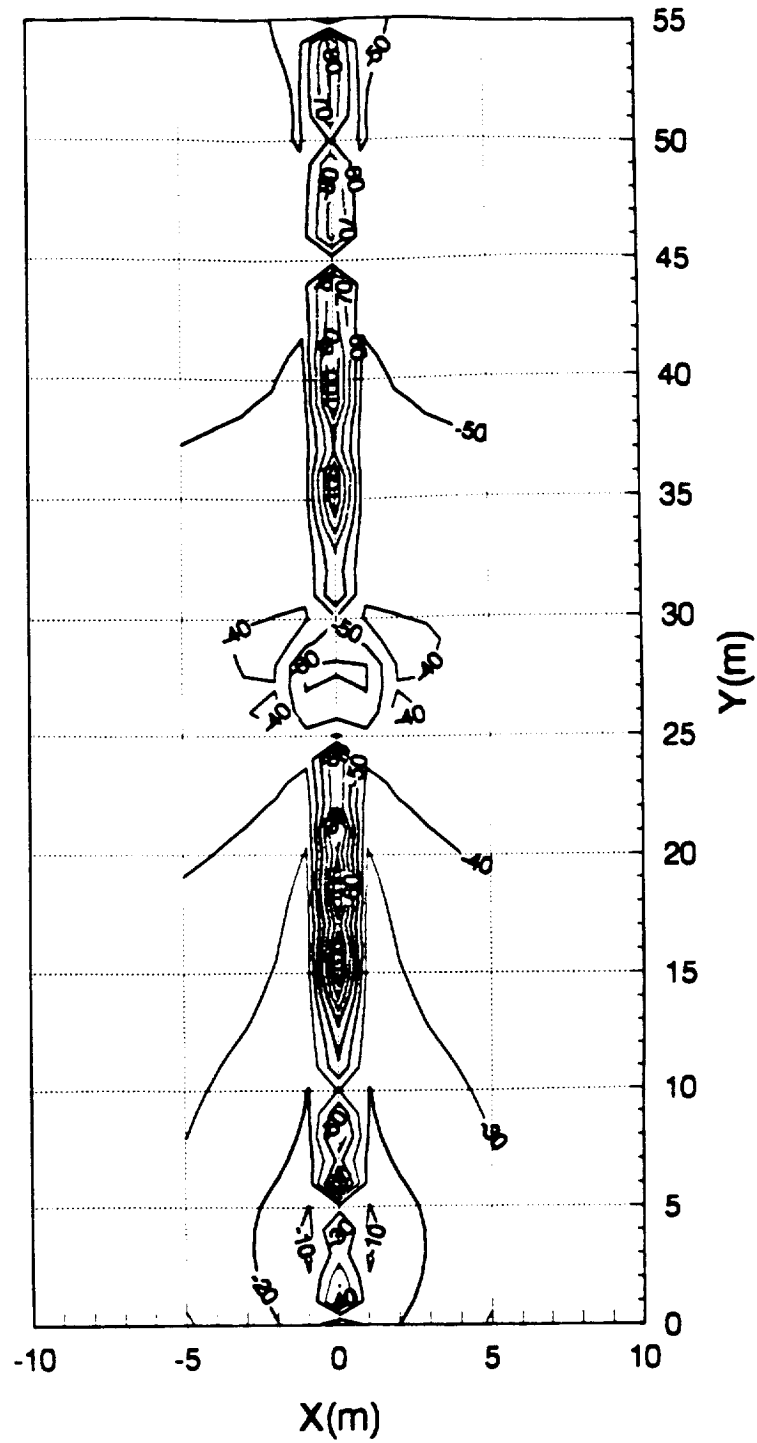
Fig. 3.11

Electric Field Intensity in Normalized dB
at 5 MHz with X = 0 (720 seg model/Source at Pos 1)
(Max = 0.325 V/m)
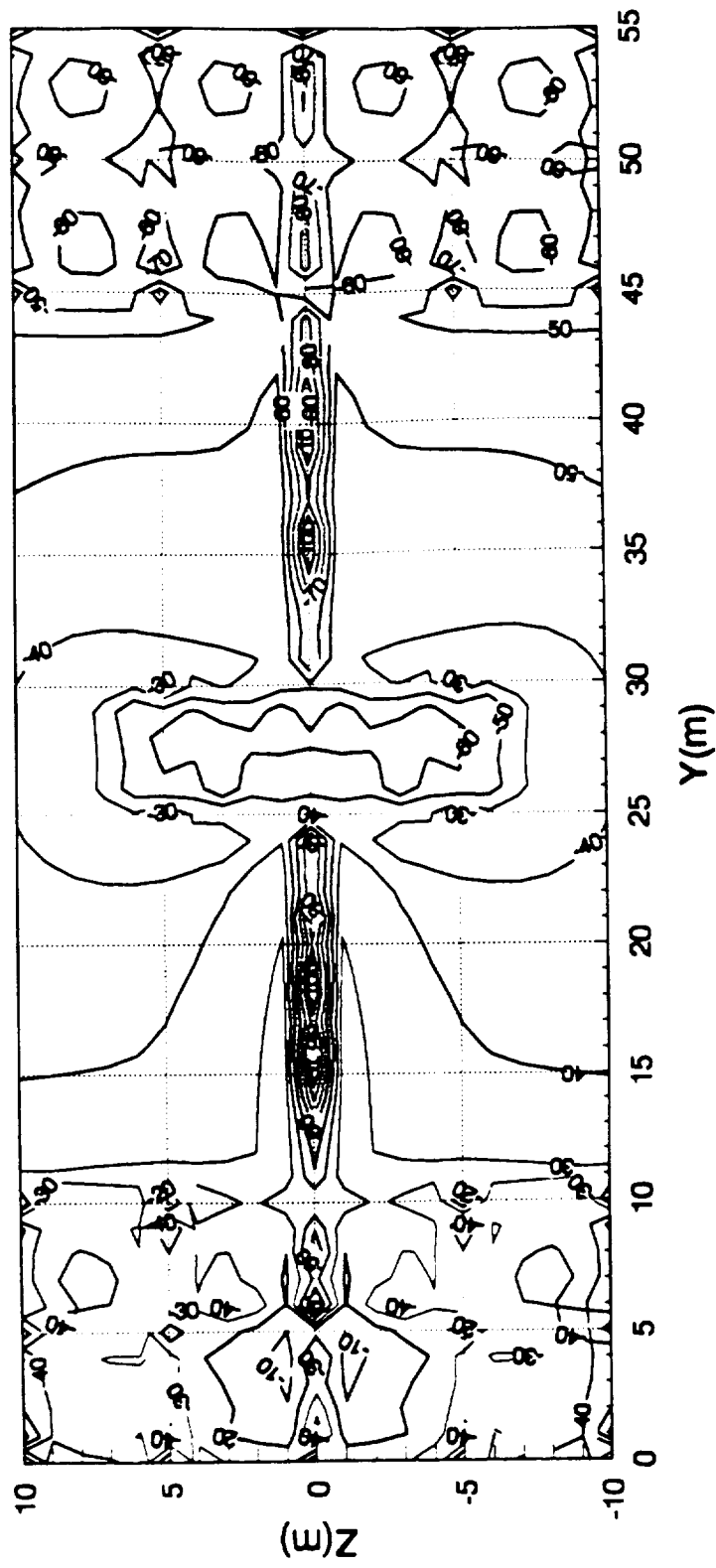
Fig. 3.12

Electric Field Intensity in Normalized dB
at 20 kHz with Z = 0 (720 seg model/Source at Pos 1)
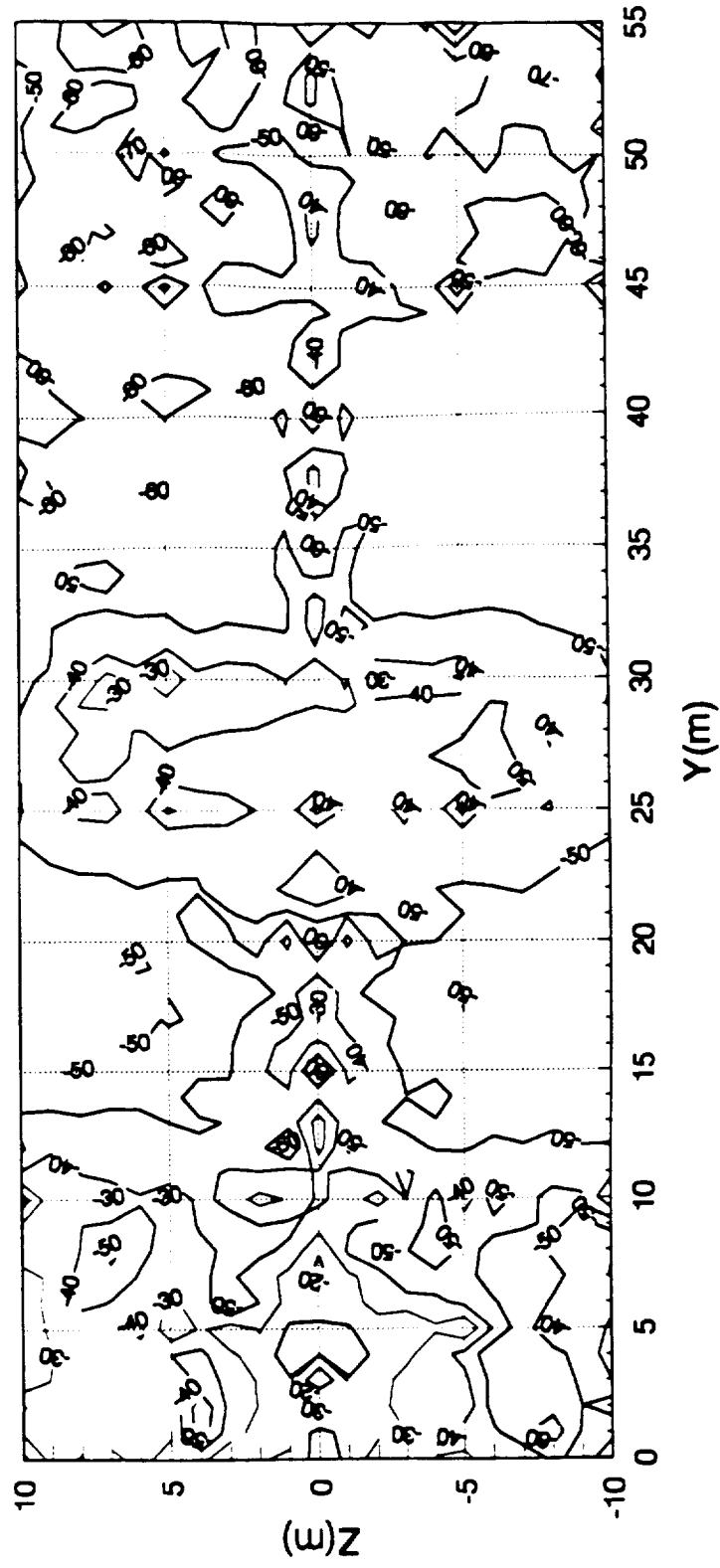(Max = 0.470 V/m)

Fig. 3.13

X(m)

Y(m)

Electric Field Intensity in Normalized dB
at 20 kHz with X = 0 (720 seg model/Source at Pos 1)
(Max = 0.470 V/m)

Fig. 3.14

Electric Field Intensity in Normalized dB
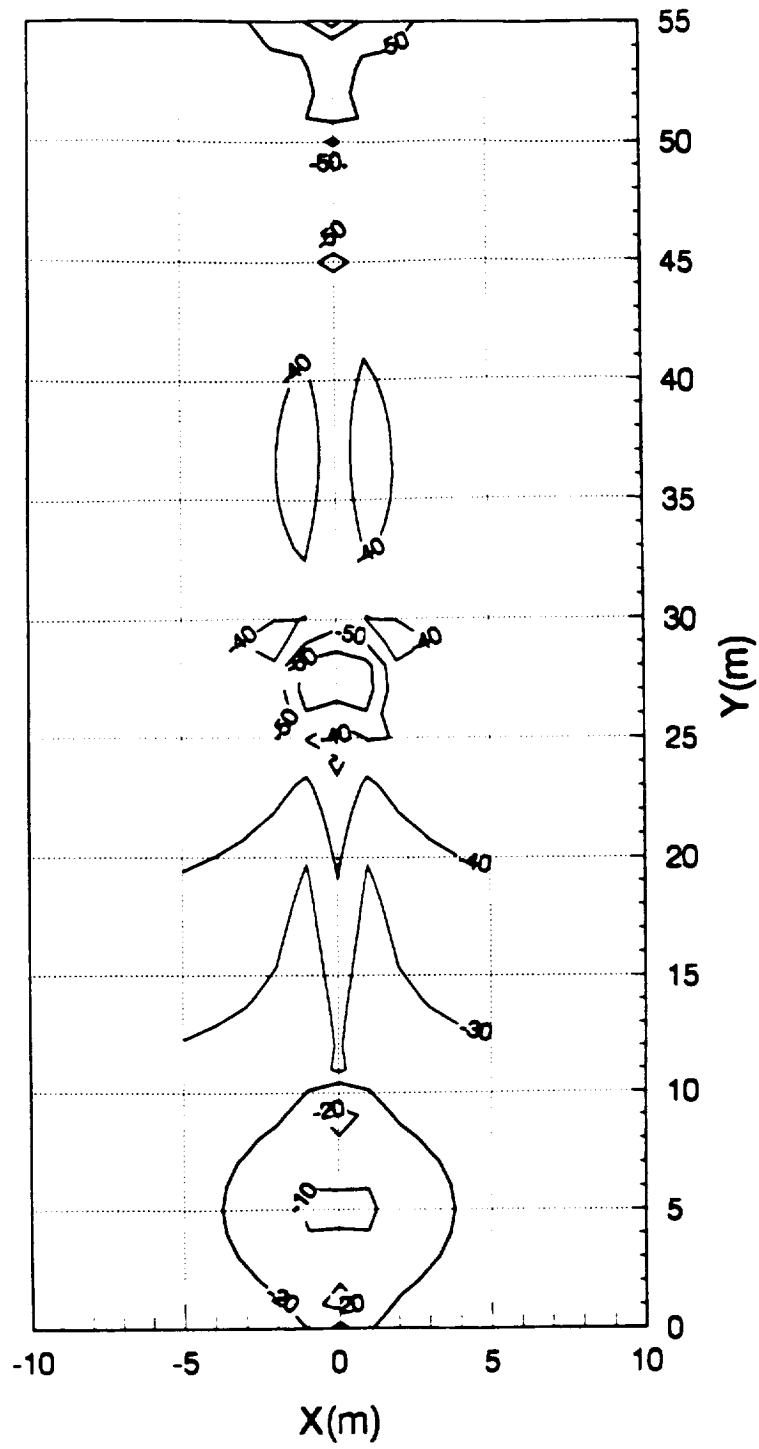at 5 MHz with Z = 0 (720 seg model/Source at Pos 2)
(Max = 0.241 V/m)

Fig. 3.15

Electric Field Intensity in Normalized dB
at 5 MHz with X = 0 (720 seg model/Source at Pos 2)
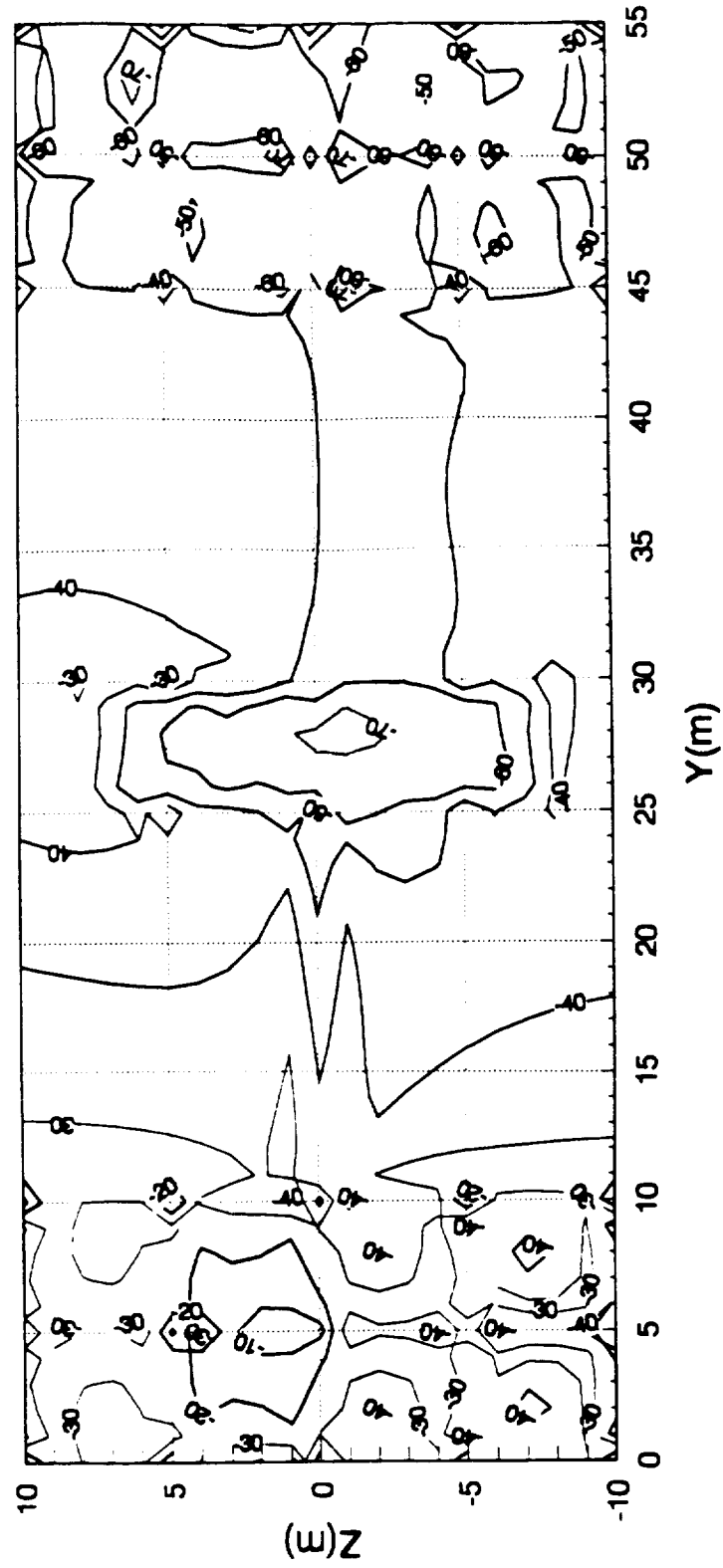(Max = 0.509 V/m)

Fig. 3.16

Electric Field Intensity in Normalized dB
at 20 kHz with Z = 0 (720 seg model/Source at Pos 2)
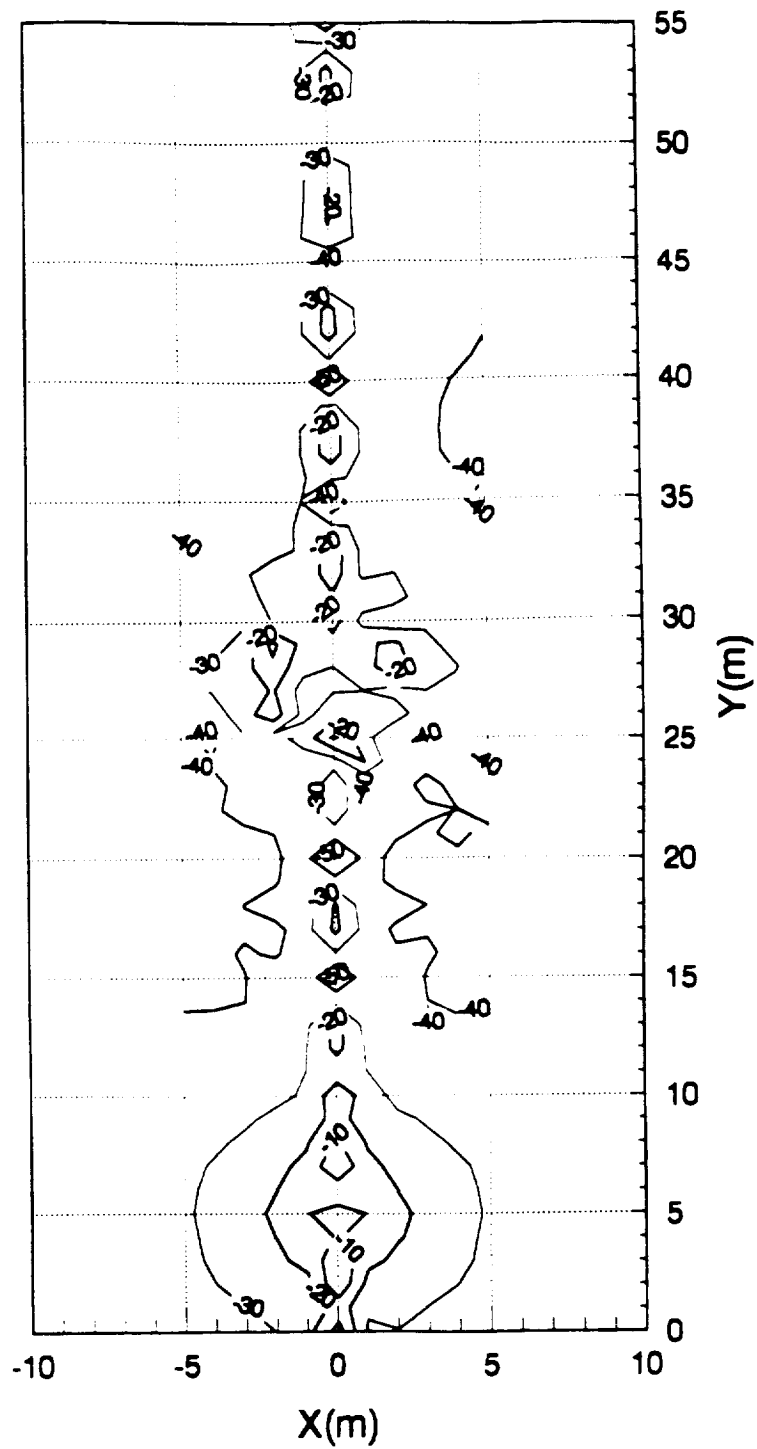(Max = 0.306 V/m)

Fig. 3.17

Electric Field Intensity in Normalized dB
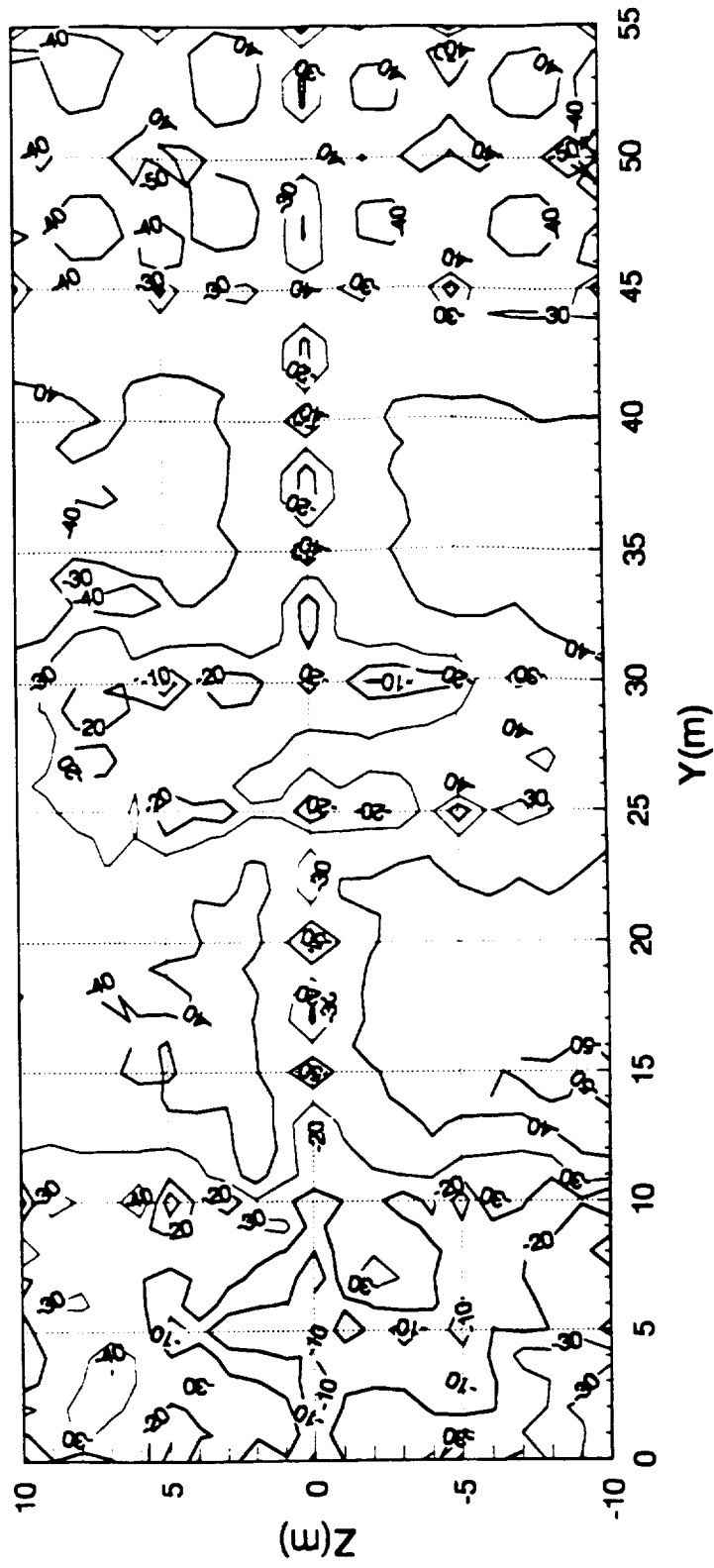at 20 kHz with X = 0 (720 seg model/Source at Pos 2)
(Max = 0.342 V/m)

Fig. 3.18

Electric Field Intensity in Normalized dB
at 5 MHz with Z = 0 (720 seg model/Source at Pos 3)
(Max = 0.00854 V/m)

Fig. 3.19

Electric Field Intensity in Normalized dB
at 5 MHz with X = 0 (720 seg model/Source at Pos 3)
(Max = 0.0288 V/m)

Fig. 3.20

File C5M_S3

Electric Field Intensity in Normalized dB
at 20 kHz with Z = 0 (720 seg model/Source at Pos 3)
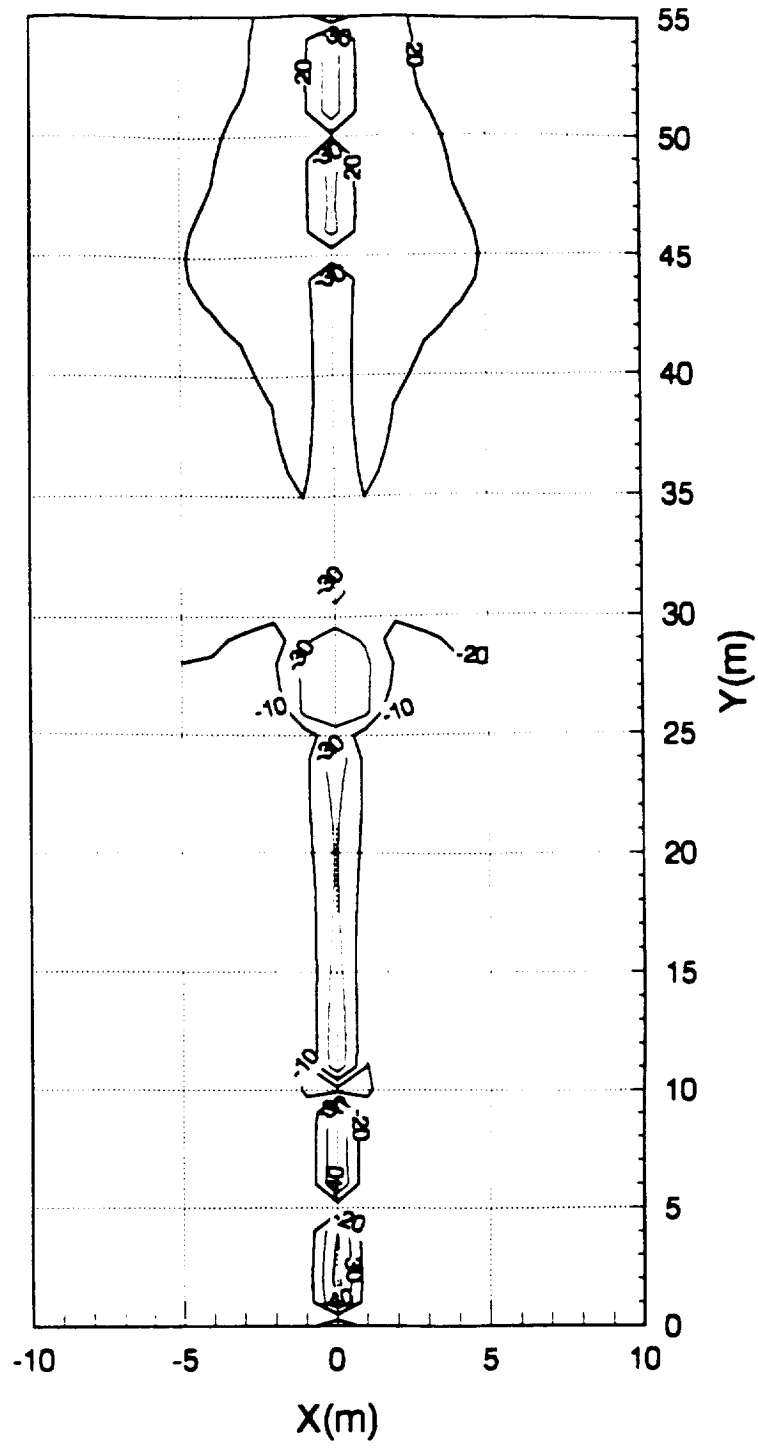(Max = 0.00664 V/m)

Fig. 3.21

Electric Field Intensity in Normalized dB
at 20 kHz with X = 0 (720 seg model/Source at Pos 3)
(Max = 0.0261 V/m)

Fig. 3.22

Electric Field Intensity in Normalized dB
at 5 MHz with Z = 0 (720 seg model/Source at Pos 4)
(Max = 0.0817 V/m)

Fig. 3.23

Electric Field Intensity in Normalized dB
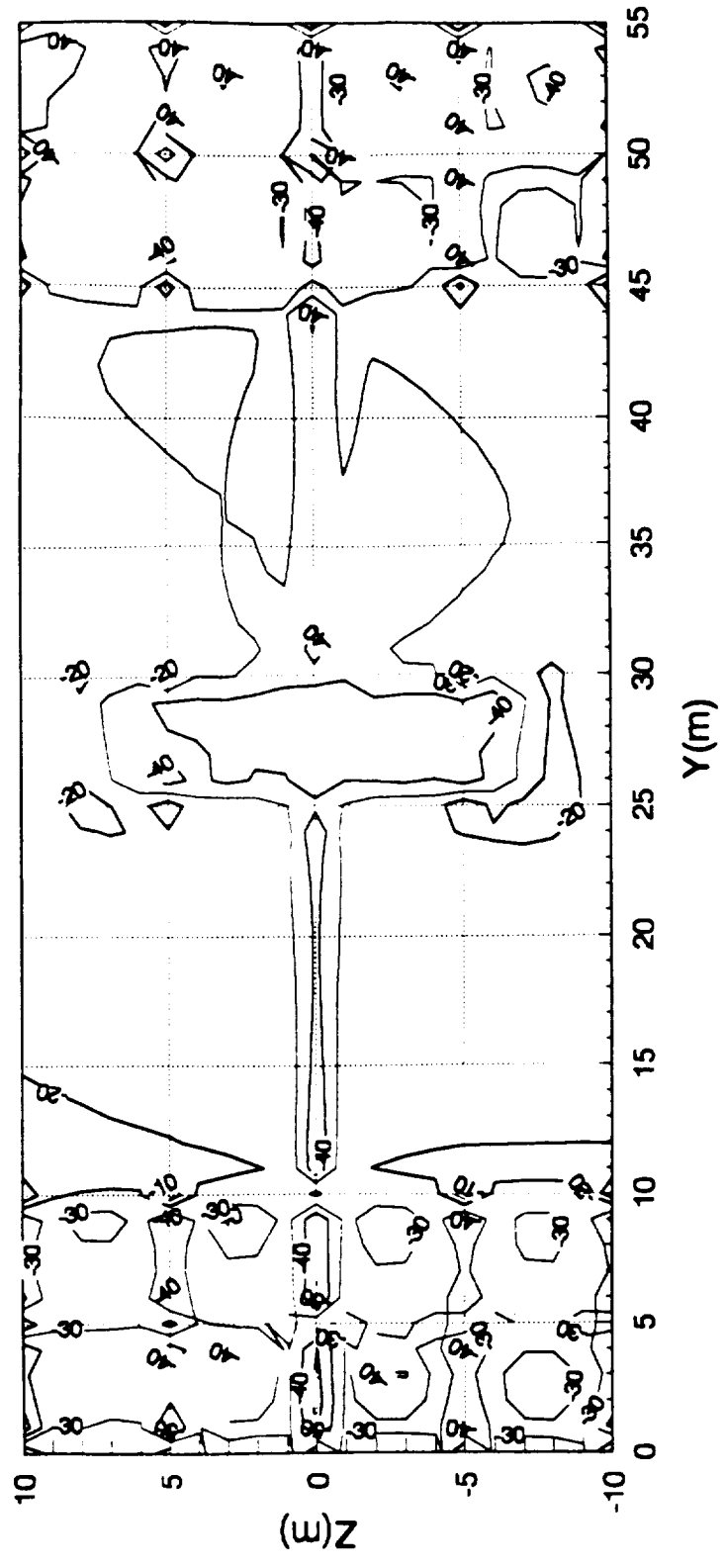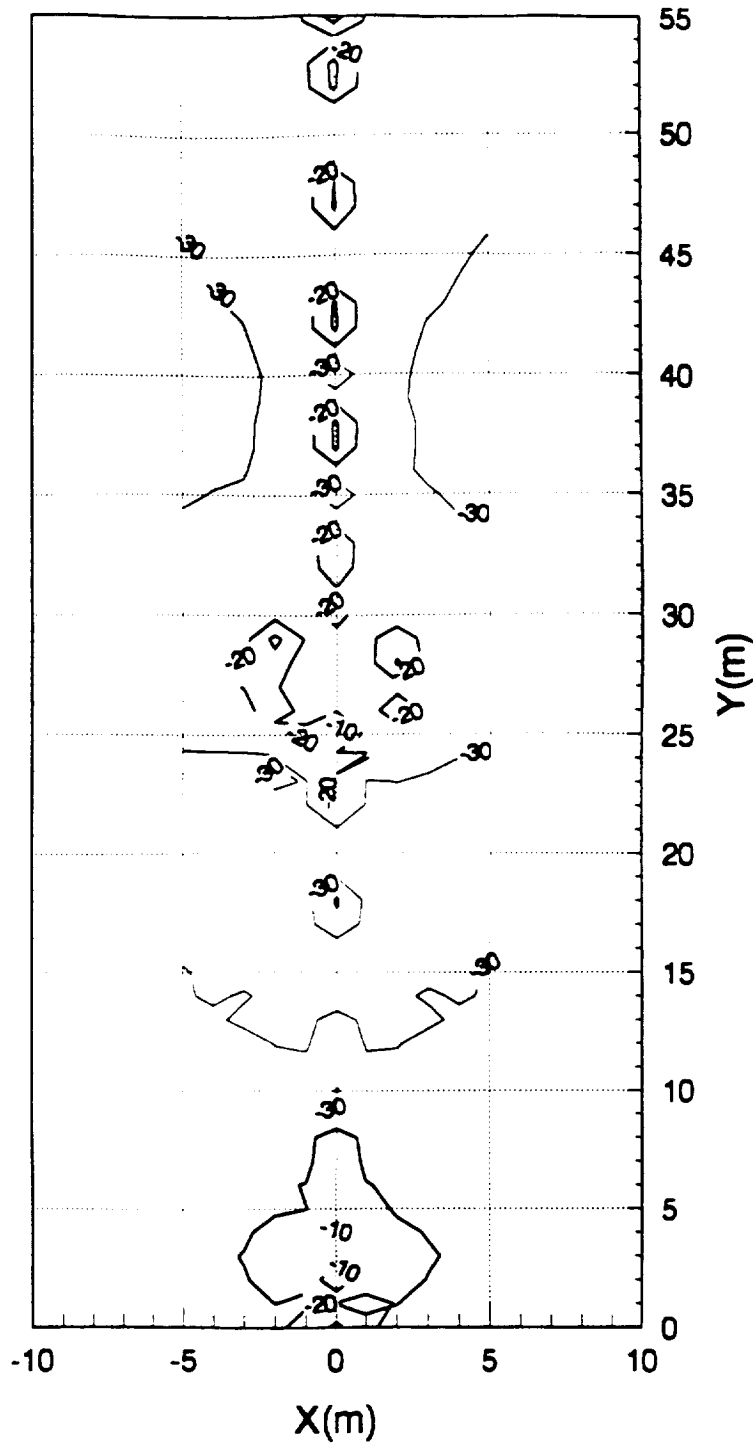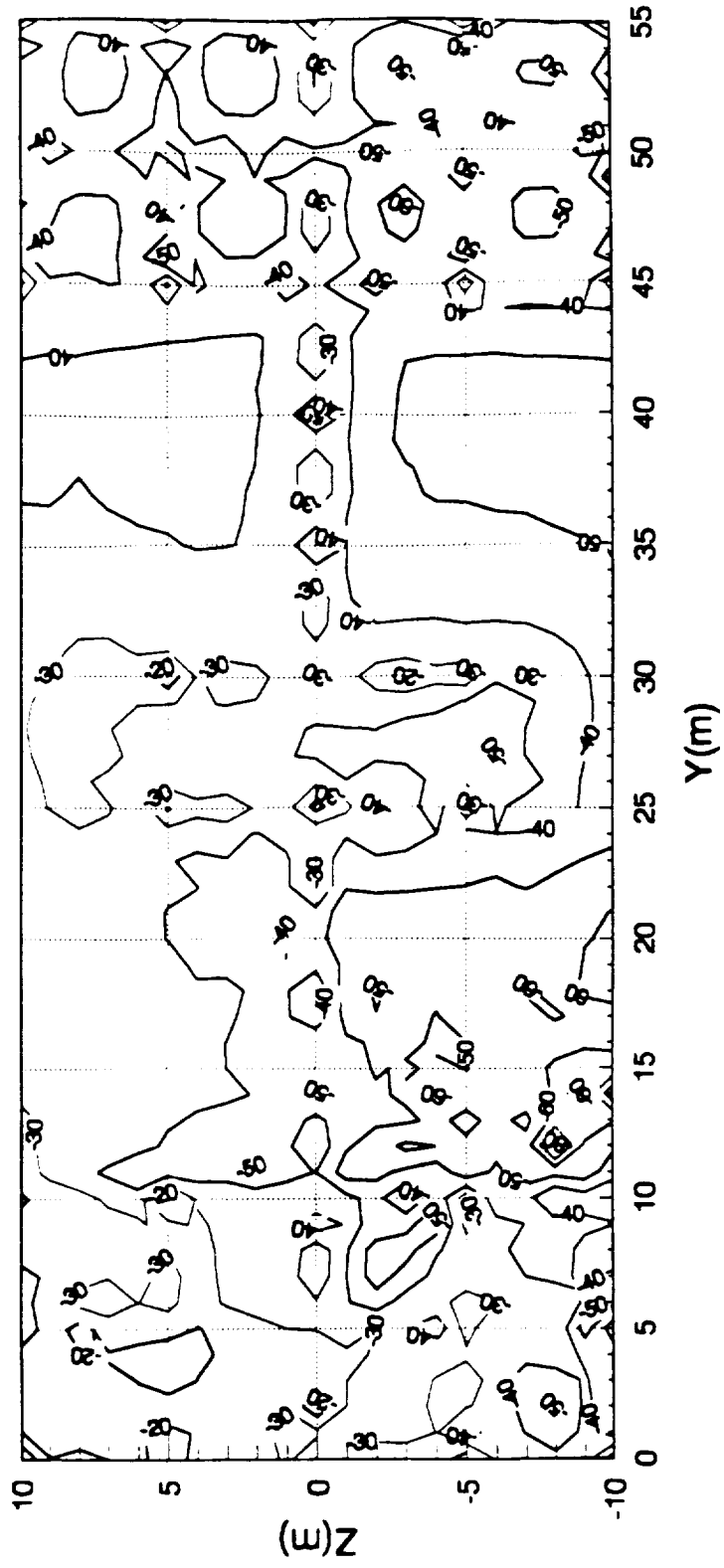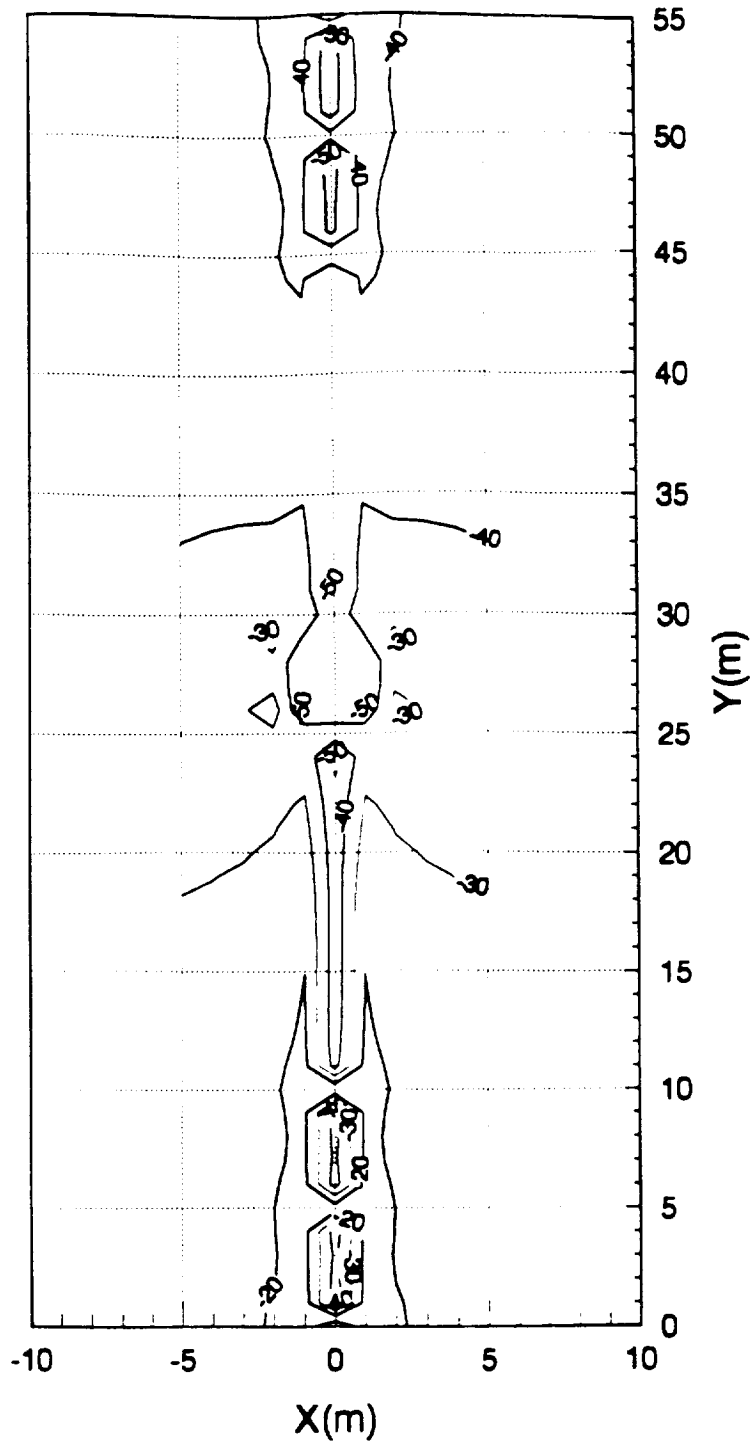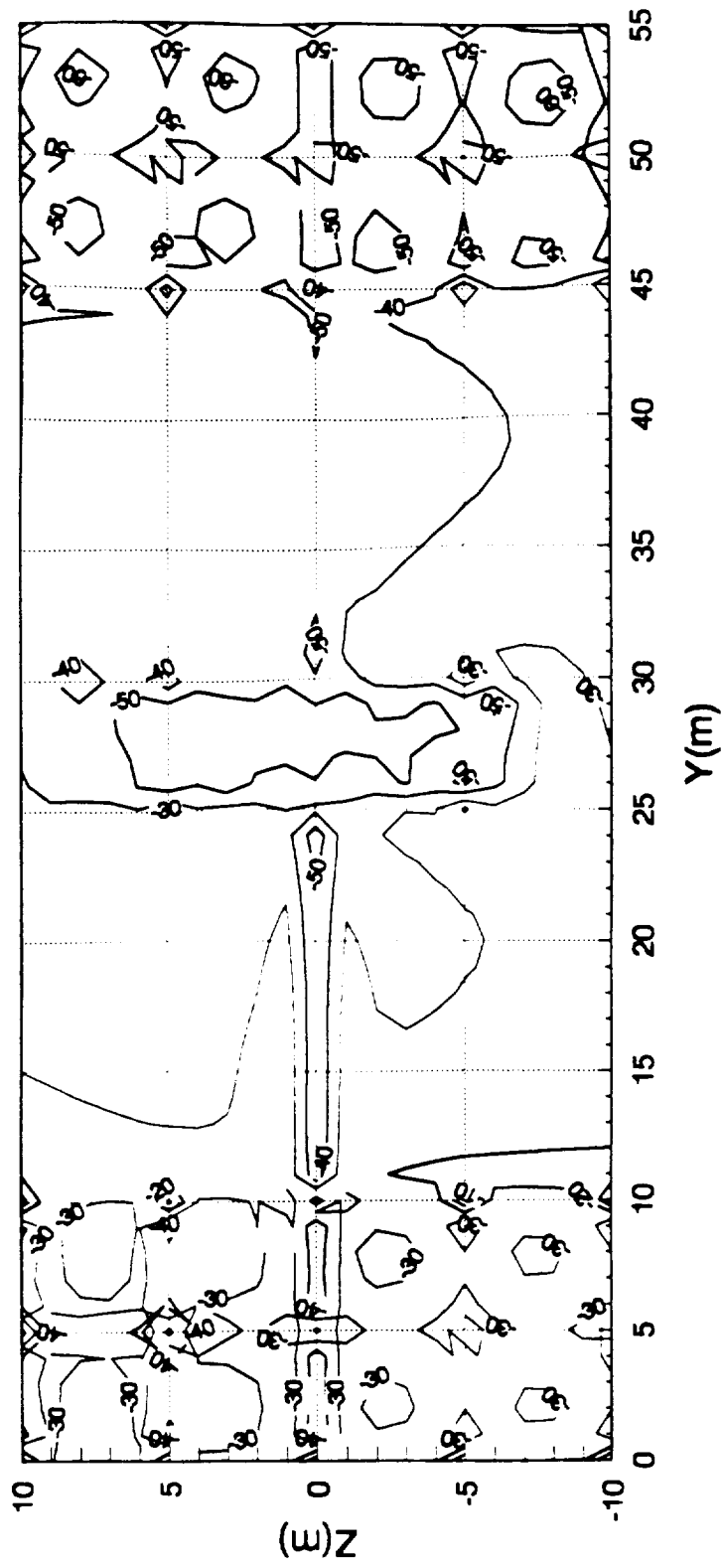at 5 MHz with X = 0 (720 seg model/Source at Pos 4)
(Max = 0.116 V/m)

Fig. 3.24

Electric Field Intensity in Normalized dB
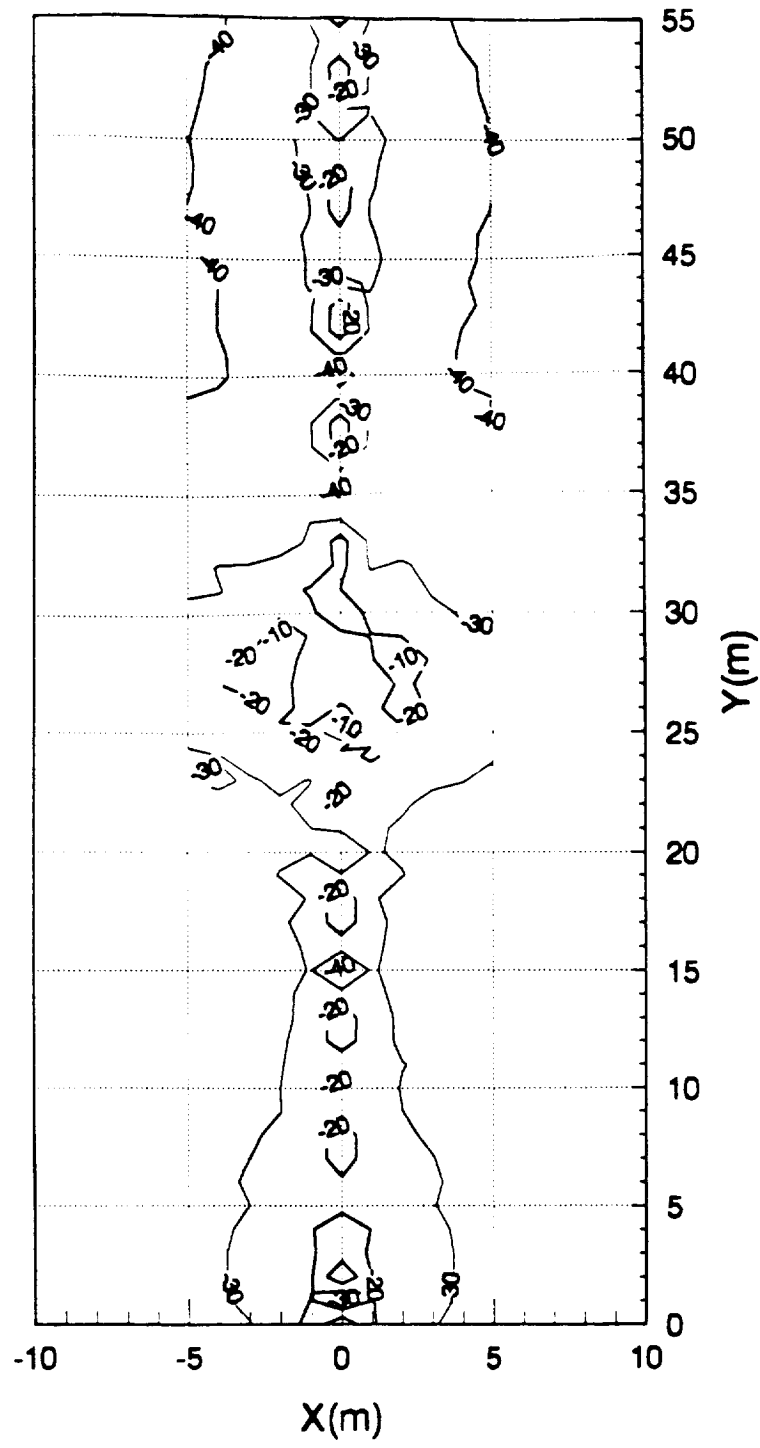at 20 kHz with Z = 0 (720 seg model/Source at Pos 4)
(Max = 0.0189 V/m)

Fig. 3.25

File C20_T4

Electric Field Intensity in Normalized dB
at 20 kHz with X = 0 (720 seg model/Source at Pos 4)
(Max = 0.0390 V/m)
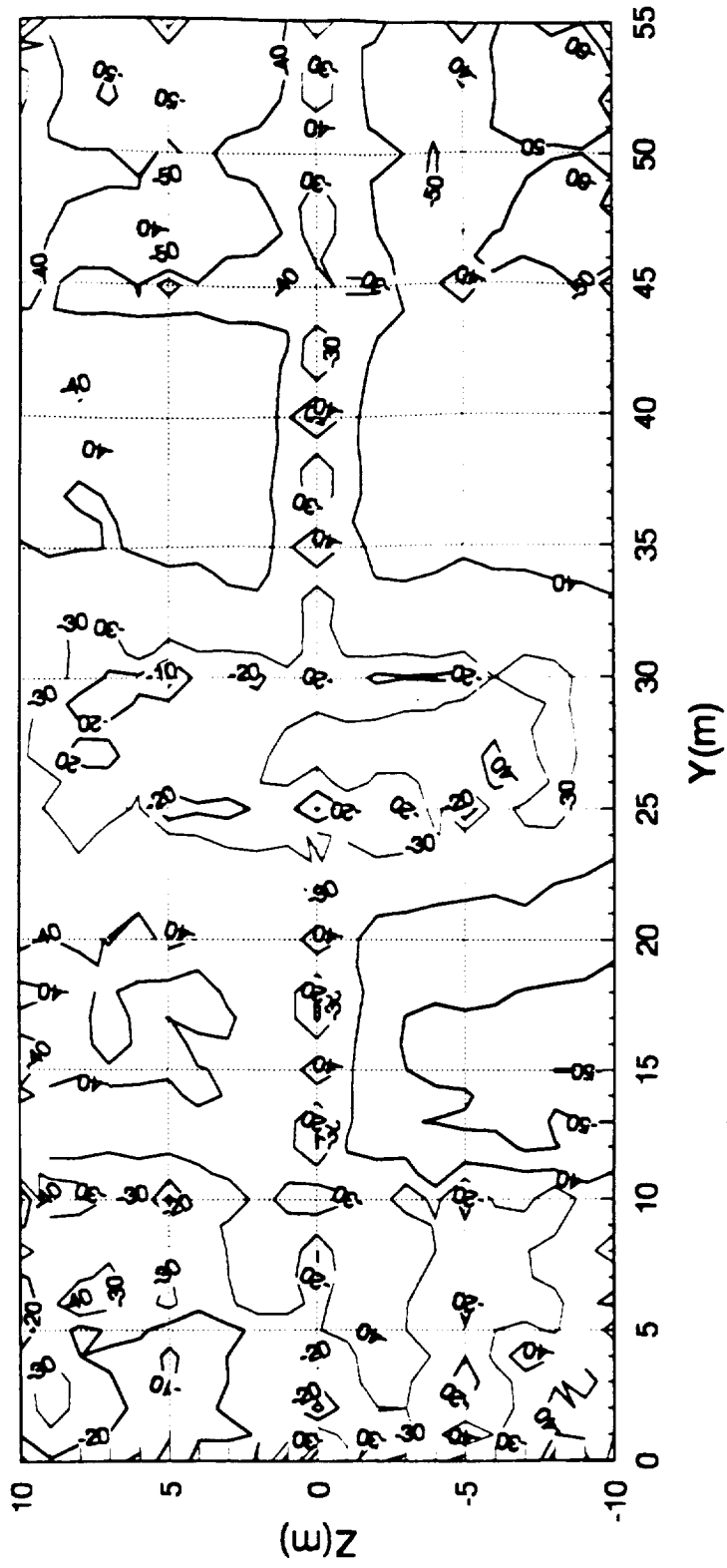
Fig. 3.26

Table 3.1 Key to Wire-Grid Graphics Files

File C5M_T1	5 MHz	Top view	Source at location 1
File C5M_S1	5 MHz	Side view	Source at location 1
File C20_T1	20 KHz	Top view	Source at location 1
File C20_S1	20 KHz	Side view	Source at location 1
File C5M_T2	5 MHz	Top view	Source at location 2
File C5M_S2	5 MHz	Side view	Source at location 2
File C20_T2	20 KHz	Top view	Source at location 2
File C20_S2	20 KHz	Side view	Source at location 2
File C5M_T3	5 MHz	Top view	Source at location 3
File C5M_S3	5 MHz	Side view	Source at location 3
File C20_T3	20 KHz	Top view	Source at location 3
File C20_S3	20 KHz	Side view	Source at location 3
File C5M_T4	5 MHz	Top view	Source at location 4
File C5M_S4	5 MHz	Side view	Source at location 4
File C20_T4	20 KHz	Top view	Source at location 4
File C20_S4	20 KHz	Side view	Source at location 4

Appendix I

J. J. Laurin, G. A. Morin, and K. G. Balmain, "Sheath wave propagation in a magnetoplasma," Radio Science **24**, pp. 289-300, 1989.

Sheath wave propagation in a magnetoplasma

J.-J. Laurin, G. A. Morin,[1] and K. G. Balmain

Department of Electrical Engineering, University of Toronto, Toronto, Ontario, Canada

A theory is presented for propagation of electromagnetic waves concentrated in the vacuum-gap sheath region separating a plane conductor from a cold magnetoplasma. The applied static magnetic field is parallel to the conductor and is in the direction of wave propagation. The theory predicts propagation at all frequencies between zero and the upper-hybrid frequency divided by $\sqrt{2}$. Experimental results are reported in which resonances caused by the wave reflection at the end of a thin cylindrical antenna aligned with the magnetic field are used to determine the sheath-wave dispersion relation. The effect of the antenna bias, plasma density and antenna diameter on the dispersion relation are studied experimentally and the results are compared with the plane-surface theory. In spite of the difference between the theoretical and experimental geometries, qualitative agreement is noted with respect to variations in magnetic field, plasma density, sheath thickness and antenna radius. The prediction that the presence of an applied magnetic field raises the upper sheath wave cutoff frequency has been confirmed experimentally, as well as the prediction that the presence of the sheath allows propagation above the cyclotron frequency. In particular, both theory and experiment show the existence near the cyclotron frequency of a special frequency at which the sheath-wave wave number is independent of the plasma density.

1. INTRODUCTION

It has been understood by many authors that the presence of a low electron density sheath surrounding an antenna immersed in isotropic plasma provides a propagation region for electromagnetic waves, a situation that is of particular interest at low frequencies (signal frequency $\omega <$ plasma frequency ω_p) where the ambient plasma is cut off for uniform plane waves. In this case, the metal-sheath-plasma region becomes analogous to a waveguide in which surface waves, so-called sheath waves, may be excited and propagate over sufficiently long distances to satisfy resonance conditions set by the finite dimensions of the antenna structure. The immediate result of these resonances is a significant contribution to the antenna impedance. In fact, impedance measurement of a simple monopole antenna has probably been the most popular method used so far in experimental sheath wave characterization [*Marec*, 1970; *Meyer et al.*, 1974; *Ishizone et al.*, 1970a, b, c]. Sheath waves not only affect antenna performance but also provide

[1] Now at Department of National Defence, Ottawa, Ontario.

a possible mechanism for locally generated electromagnetic waves to propagate between widely separated points on large spacecraft in the ionosphere. These waves could give rise to electromagnetic interference if picked up by sensitive devices distant from the source.

In this paper, results of theoretical and experimental research on sheath wave propagation in a magnetized plasma are presented, for the case of propagation in the direction of the static magnetic field B_0. In earlier work, *Mushiake* [1964] derived a dispersion relation for surface waves along a thin, unsheathed wire parallel to B_0. His equation predicted propagation cutoff for frequencies greater than the cylotron frequency ω_c. *Adachi* [1977] proposed a transmission line model to calculate the impedance of a sheathless dipole antenna of finite thickness oriented at an arbitrary angle with respect to B_0. In the case where the antenna and B_0 are aligned, this model predicts resonances called "lower n wavelength" below ω_c. Given the antenna length, the frequencies of these resonances can be predicted by Mushiake's formula. *Miller* [1967a, b] found that the presence of a vacuum gap sheath allows surface wave propagation (therefore called sheath-wave propagation) well above ω_c. On the experimental side, measurements done in laboratory magnetized plas-
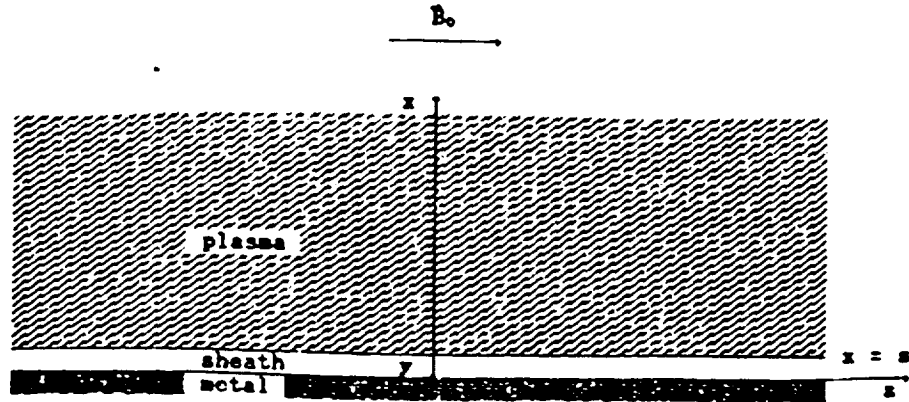
B₀

Fig. 1. Planar configuration for sheath wave propagation in the *z* direction.

mas [*Ishizone et al.*, 1969, 1970a, b; *Sawaya et al.*, 1978] have revealed the presence of one, and sometimes two, resonance peaks in the neighborhood of ω_c. Due to this small number of resonances, there is only limited evidence that their presence is related to sheath-wave propagation. This is because there could be many other types of waves that are likely to cause resonance in a finite-dimension plasma chamber. Also, even if the resonances reported were due to sheath waves, their small number would make difficult, if not impossible, the study of the dispersion relation.

The objective of the present work is to establish clear experimental evidence that sheath waves indeed exist on an antenna in a magnetoplasma, that the waves can be easily excited, and that their dispersion relation can be determined approximately through measurement of antenna input impedance. A further objective is to relate the measured dispersion relation to the theoretical relation for sheath waves in a planar plasma-sheath-conductor region.

2. THEORY

The derivation of the dispersion relation of surface waves propagating over an infinite metal structure immersed in a magnetoplasma is now given. In order to simplify the problem from a mathematical and computational point of view, the following geometry has been adopted. The metal structure is reduced to an infinite plane over which is a semi-infinite magnetoplasma. A vacuum sheath of arbitrary thickness separates the metal from the plasma (see Figure 1).

The study has also been limited to the particular case where the metal surface and the direction of propagation are parallel to the magnetic field which

is in the *z* direction. In fact, it is the only situation in which the planar geometry is comparable to the cylindrical one in which we are actually interested. In the general case, the angle between the normal to the surface and **B₀** is not constant around a cylindrical surface, a situation that is impossible to reproduce with a planar structure. This incompatibility is avoided if the cylinder considered is aligned with **B₀**.

Finally, any variation of the field quantities in the *ŷ* direction is neglected. This will not only simplify the analysis but also will provide similarity between the anticipated solution for the plane and the case of the cylindrical geometry in which azimuthal symmetry would be assumed.

For the plasma region, a cold magnetoplasma of uniform density was assumed. In this model, the relative permittivity is given by the well known tensor:

$$K = \begin{bmatrix} K' & jK^* & 0 \\ -jK^* & K' & 0 \\ 0 & 0 & K_0 \end{bmatrix} = \mathcal{E}_r \qquad (1)$$

in which

$$K' = 1 - \frac{UX}{U^2 - Y^2} \qquad K^* = \frac{-YX}{U^2 - Y^2}$$

$$K_0 = 1 - \frac{X}{U} =$$

with

$$X = \omega_p^2/\omega^2 \qquad Y = \omega_c/\omega \qquad U = 1 - jv\,\omega$$

ω_p electron plasma frequency;
ω_c electron cyclotron frequency;
ω excitation frequency;
v effective electron-neutral collision frequency.

The SI system of units has been adopted in this paper. Also, all the field quantities, except B_0, will be manipulated as phasors.

In the case of harmonic time dependence of the type $e^{j\omega t}$, Maxwell's equations are written

$$\nabla \times H = j\omega\varepsilon_0 K \cdot E \qquad (2a)$$

$$\nabla \times E = -j\omega\mu_0 H \qquad (2b)$$

$$\nabla \cdot K \cdot E = 0 \qquad (2c)$$

$$\nabla \cdot H = 0 \qquad (2d)$$

for the plasma region, and

$$\nabla \times H = j\omega\varepsilon_0 E \qquad (3a)$$

$$\nabla \times E = -j\omega\mu_0 H \qquad (3b)$$

$$\nabla \cdot E = 0 \qquad (3c)$$

$$\nabla \cdot H = 0 \qquad (3d)$$

in the vacuum-gap sheath region. Assuming a z variation of the type e^{-kz}, where k is the complex propagation constant, one can write the ∇ operator as

$$\nabla = \left(\frac{\partial}{\partial x} \hat{x}, 0\hat{y}, -jk\hat{z}\right)$$

2.1. Solution in the sheath

Using this definition of ∇, the components of E and H can be conveniently separated into two independent sets and the general solution to equations (3) is written as a superposition of a TM and a TE mode:

TM mode

$$H_y = C \cosh(hx) + E \sinh(hx) \qquad (4a)$$

$$E_z = \frac{k}{\omega\varepsilon_0} H_y \qquad (4b)$$

$$E_x = \frac{h}{j\omega\varepsilon_0}(C \sinh(hx) + E \cosh(hx)) \qquad (4c)$$

TE mode

$$E_y = D \sinh(hx) + F \cosh(hx) \qquad (5a)$$

$$H_z = \frac{-k}{\omega\mu_0} E_y \qquad (5b)$$

$$H_x = \frac{-h}{j\omega\mu_0}(D \cosh(hx) + F \sinh(hx)) \qquad (5c)$$

where

$$h = (k^2 - \beta_0^2)^{1/2} \qquad (5d)$$

in which $\beta_0^2 = \omega^2\varepsilon_0\mu_0$. C, D, E and F are arbitrary constants. The boundary conditions at the metal surface ($x = 0$) require that $E_y = 0$ and $E_z = 0$. This sets $E = F = 0$ in (4) and (5).

2.2. Solution in the plasma

Unlike the sheath region, the anisotropic nature of the plasma makes impossible the separation of the field components into two independent sets. Therefore it is only necessary to solve for one field component from which all the others can be derived. The choice of this field component may seem purely arbitrary a priori. The choice of a component belonging to the TM mode will lead to a more general solution because, as it will be seen later, the components of the TE wave vanish if ω_c is reduced to 0. Also, in order to ensure conformity with the existing literature, the solution for E_z is found.

After a few algebraic manipulations [Laurin, 1986], equations (2) can be combined into the following:

$$(\nabla_t^2 - x_1^2)(\nabla_t^2 - x_2^2)E_z = 0 \qquad (6)$$

where ∇_t is the component of ∇ perpendicular to the $\hat{z}$ direction. The quantities x_1^2 and x_2^2 are solutions of the biquadratic equation,

$$ax^4 + bx^2 + c = 0 \qquad (7a)$$

with

$$a = K' \qquad (7b)$$

$$b = \beta_0^2(K'^2 - K^{-2} + K'K_0) - k^2(K_0 + K') \qquad (7c)$$

$$c = \beta_0^4 K_0(K'^2 - K^{-2}) - 2\beta_0^2 k^2 K_0 K' + k^4 K_0 \qquad (7d)$$

With $\nabla_t = (\partial/\partial x)\hat{x}$, the general solution to (6) is

$$E_z = Ae^{x_1 x} + Be^{-x_1 x} + Ge^{-x_2 x} + Ie^{-x_2 x}$$

A, B, G and I are constants. If we choose x_1 and x_2 such that their real parts are negative, the solution for E_z remains physically possibly only if $G = I = 0$. Thus,

$$E_z = Ae^{x_1 x} + Be^{x_2 x} \qquad (8)$$

However, in the particular case where

$$b^2 - 4ac = 0 \qquad (9)$$

the general solution for E_z is

$$E_z = (Ax + B)e^{x x} \qquad (10)$$

with

$$x = -\left(\frac{-b}{2a}\right)^{1/2}$$

For this last solution, k can be obtained directly from (9) and it is independent of the sheath thickness. However, calculation of the fields in the sheath and in the plasma using this value of k reveals that all the boundary conditions at the sheath edge cannot be satisfied simultaneously. This second type of solution should therefore be rejected.

For the solution given by (8), the other field components are easily calculated by putting E_z back into Maxwell's equations.

$$E_z = \frac{j}{kK'}\left[\frac{(k^2K_0 - \varphi)}{\alpha_1}Ae^{\alpha_1 x} + \frac{(k^2K_0 - \theta)}{\alpha_2}Be^{\alpha_2 x}\right]$$

$$E_y = \frac{1}{kK'}\left(\frac{\varphi}{\alpha_1}Ae^{\alpha_1 x} + \frac{\theta}{\alpha_2}Be^{\alpha_2 x}\right)$$

$$H_x = \frac{-1}{K'\omega\mu_0}\left(\frac{\varphi}{\alpha_1}Ae^{\alpha_1 x} + \frac{\theta}{\alpha_2}Be^{\alpha_2 x}\right)$$

$$H_y = j\omega\varepsilon_0 K_0\left(\frac{A}{\alpha_1}e^{\alpha_1 x} + \frac{B}{\alpha_2}e^{\alpha_2 x}\right)$$

$$H_z = \frac{j}{kK'\omega\mu_0}(\varphi Ae^{\alpha_1 x} + \theta Be^{\alpha_2 x})$$

where

$$\varphi = K_0(k^2 - \beta_0^2 K') - K'\alpha_1^2$$

$$\theta = K_0(k^2 - \beta_0^2 K') - K'\alpha_2^2$$

2.3. Dispersion relation for the sheath waves

The dispersion relation is obtained from the boundary conditions at the sheath-plasma interface which are (1) absence of charge accumulation other than polarization charges and (2) absence of surface current (electric and magnetic). Those conditions are satisfied if, at $x = s$, (1) D_x is continuous:

$$\frac{C}{\omega\varepsilon_0}\cosh(hs) = jK_0\left(\frac{A}{\alpha_1}e^{\alpha_1 s} + \frac{B}{\alpha_2}e^{\alpha_2 s}\right) \quad (11a)$$

(2) E_y is continuous:

$$D\sinh(hs) = \frac{1}{k}\left(\frac{\varphi}{\alpha_1}Ae^{\alpha_1 s} + \frac{\theta}{\alpha_2}Be^{\alpha_2 s}\right) \quad (11b)$$

(3) E_z is continuous:

$$\frac{h}{j\omega\varepsilon_0}C\sinh(hs) = Ae^{\alpha_1 s} + Be^{\alpha_2 s} \quad (11c)$$

(4) H_x is continuous (satisfied by case 2), (5) H_y is continuous (satisfied by case 1), and (6) H_z is continuous:

$$hD\cosh(hs) = \frac{1}{k}(\varphi Ae^{\alpha_1 s} + \theta Be^{\alpha_2 s}) \quad (11d)$$

Note that in equations (11b) and (11d), the previous constant D has been arbitrarily replaced by D/K'. This substitution facilitates the use of the same derivation for the solution in the isotropic case by simply setting $\omega_c = 0$ in the expressions for the fields. When $\omega_c = 0$, we have $K' = K_0$ and $K'' = 0$ and equations (7) can then be combined to form

$$(\alpha^2 + \beta_0^2 K_0 - k^2)^2 = 0$$

or

$$\alpha_1^2 = \alpha_2^2 = \alpha^2 = k^2 - \beta_0^2 K_0$$

which leads to

$$\varphi = \theta = 0$$

Also, the general solution for E_z in the plasma region becomes

$$E_z = Ae^{\alpha x} \quad (12)$$

Equations (11a), (11b), and (11c) are then equivalent to, respectively,

$$C\cosh(hs) = \frac{j\omega\varepsilon_0 K_0}{\alpha}Ae^{\alpha s} \quad (13a)$$

$$D = 0 \quad (13b)$$

$$C\sinh(hs) = \frac{j\omega\varepsilon_0}{h}Ae^{\alpha s} \quad (13c)$$

Elimination of the constants A and C gives the dispersion relation for the isotropic case:

$$\tanh(hs) = \frac{\alpha}{K_0 h}$$

When there is no sheath, the boundary condition on E_z at the metal surface sets $A = 0$ in (12), which makes all the fields vanish. This differs from the sheathless anisotropic case where the boundary condition on E_z (given by (8)) sets $A = -B$, resulting in nonvanishing fields.

For the anisotropic case, the elimination of the constants A, B, C, and D leads to the dispersion relation

$$\tanh^2(hs)(\theta\alpha_2 - \varphi\alpha_1) + \frac{\theta\alpha_1 - \varphi\alpha_2}{K_0}$$
$$+ \tanh(hs)(\varphi - \theta)\left(\frac{\alpha_1\alpha_2}{hK_0} + h\right) = 0 \quad (14)$$